Tunneling Splittings for "O···O Stretching" and Other Vibrations of Tropolone Isotopomers Observed in the Infrared Spectrum Below 800 cm^{-1}

Richard L. Redington* and Theresa E. Redington

Department of Chemistry and Biochemistry, Texas Tech University, Lubbock, Texas 79409

Robert L. Sams

Wiley Environmental Molecular Sciences Laboratory, Pacific Northwest National Laboratory, Richland, Washington 99352

Received: July 20, 2007; In Final Form: November 2, 2007

Fourier transform infrared absorption spectra containing evidence for about two dozen spectral tunneling doublets are reported for gaseous tropolone(OH), tropolone (OD), and ^{18}O,^{18}O-tropolone(OH) in the 800 to 300 cm^{-1} spectral range. No FTIR absorption was detected in the 300−150 cm^{-1} range. The known zero-point (ZP) tunneling splitting values $\Delta_0 = 0.974$ cm^{-1} for tropolone(OH) (Tanaka et al.) and 0.051 cm^{-1} for tropolone(OD) (Keske et al.) allow vibrational state-specific tunneling splittings Δ_v to be estimated for fundamentals including three with strong O···O stretching displacements [cf. for tropolone(OH) $\nu_{13}(a_1) =$ 435.22 cm^{-1} with $^{H}\Delta_{13} = 1.71$ $cm^{-1} = 1.76$ $^{H}\Delta_0$, and for tropolone(OD) $\nu_{13}(a_1) = 429.65$ cm^{-1} with $^{D}\Delta_{13} =$ 0.32 $cm^{-1} = 6.27$ $^{D}\Delta_0$]. The majority of Δ_v splittings in the sub-800 cm^{-1} range are dilated relative to the isotopomer Δ_0 values. The FTIR spectra demonstrate the presence of dynamic couplings and potential function anharmonicity in addition to revealing Δ_v splittings and many OH/D and $^{18}O/^{16}O$ isotope effects. Approximate values are obtained for the ZP splittings $^{88}\Delta_0$ and $^{86}\Delta_0$ of the doubly and singly ^{18}O-labeled isotopomers of tropolone(OH). The diverse values of the observed Δ_v/Δ_0 splitting ratios underscore the inherent multidimensionality and corner-cutting activities entering the state-specific tunneling processes of the tropolone tautomerization reaction.

1. Introduction

Tropolone, 2-hydroxy-2,4,6-cycloheptatrien-1-one, has an equal double-minimum multidimensional potential energy surface (PES) allowing its two equivalent tautomers to interconvert as shown in Figure 1. Its PES has properties that permit the spectroscopic observation of many state-specific tunneling doublets.[1−10] Fourier transform infrared (FTIR) absorption spectroscopy at spectral resolutions reaching 0.0025 cm^{-1} was previously used to study gaseous tropolone(OH) [Tp(OH)][11−13] and its ^{18}O-labeled isotopomers[14] in spectral ranges above 700 cm^{-1}. The congested individual rotational transitions of gaseous Tp at room temperature are not resolved at 0.0025 cm^{-1} resolution. This is, however, needed in order to study the sharp Q branch structures marking the approximate origins for many spectral tunneling doublets. The first spectral doublets observed for excited vibrations of Tp(OD) and for the lower frequency Tp(OH) vibrations are reported here. The spectra also contain evidence for nonharmonic potential and kinetic energy couplings which particularly affect the IR absorption strengths. As noted previously for Tp(OH),[13] the density of rotation-contortion-vibration background states developed with vibrations $\nu_v > 800$ cm^{-1} appears to reach critical values permitting intramolecular vibrational energy redistribution (IVR) processes to occur. When these processes are fast on the time scale of the zero-point (ZP) tautomerization rate, they attenuate the influence of a vibrational excitation on the tunneling splitting value.

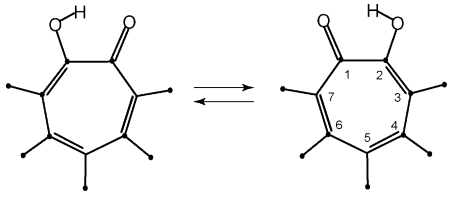

Figure 1. Interchange of equivalent tautomer structures for tropolone, $C_7H_6O_2$.

The FTIR spectra of gaseous Tp[OH(OD)] between 800 and 150 cm^{-1} are reported. Analysis of the Tp(OD) data utilizes the precise ZP splitting value $^{D}\Delta_0 = 1523.227(5)$ MHz recently obtained by Keske et al.[9] through FT microwave spectroscopy on jet-cooled samples. The new FTIR spectral information, summarized in Tables 1−4, shows that several previously proposed vibrational assignments[11−16] for Tp[OH(OD)] are incorrect. The reassignments include transitions of Ne-isolated Tp(OH) at 754 and of Tp(OD) at 751.3 cm^{-1} previously assigned to infer a spectral doublet component separation (DS_{37}) near 10 cm^{-1} for $\nu_{37}(b_2)$ (in-plane skeletal deformation) of Tp-[OH(OD)]. Exclusive of the OH(OD) stretching fundamentals, the most dilated fundamental splittings Δ_v are expected to involve prominent O···O stretching displacements as is verified for Tp in the present work. Various theoretical approaches to the state-specific tunneling dynamics of tropolone[16−25] are considered in recent reviews.[26−27]

The FT microwave study of Keske et al.[9] produced ZP splitting values $^{iso}\Delta_0$ for the four singly labeled ^{13}C isotopomers of Tp(OH), and rotational constant values for the lower ZP state

* To whom correspondence should be addressed.

10.1021/jp0757255 CCC: $40.75
Published on Web 01/25/2008

TABLE 1: a_1 and A_1 Transitions and Tunneling Splittings of Tp Isotopomers below 800 cm^{-1}

	doublet components[a]		vibrational frequencies[b]			vib. isotope shifts[c]		tunneling effects[d]			
vib.	$\nu_{v,a}$	$\nu_{v,b}$	$\nu_{v,ave}$	ω_v	ν_v/ω_v	calc	obs	DS_v	Δ_v	Δ_v/Δ_0	R_v
				$\nu_c = \nu_{13}(a_1) + 2\nu_{26}(b_1)$ (A_1) [dilating]							
$^{66}\nu_c$	772.48	773.06	772.77	776.3	0.99	0.0	0.0	0.58	1.55	1.59	1.00
$^{D}\nu_c$	769.120	769.198	769.159	767.6	1.00	8.7	3.6	0.078	0.13	2.55	1.60
				$\nu_{12}(a_1)$ symmetrical skeletal breathing [dilating]							
$^{66}\nu_{12}$	711.28	711.35	711.32	702.7	1.01	0.0	0.0	0.07	1.04	1.07	1.00
$^{88}\nu_{12}$				692.1		10.7					
$^{D}\nu_{12}$	710.01	710.06	710.03	701.6	1.01	1.1	1.3	0.05	0.10	1.96	1.83
				$\nu_{13}(a_1)$ O···O stretching, Figure 8A [dilating]							
$^{66}\nu_{13}$	434.85	435.59	435.22	440.9	0.99	0.0	0.0	0.74	1.71	1.76	1.00
$^{88}\nu_{13}$	426.47	427.17	426.82	431.7	0.99	9.1	8.4	0.70	1.53	1.84	1.05
$^{D}\nu_{13}$	429.51	429.78	429.65	434.0	0.99	6.8	5.6	0.27	0.32	6.27	3.56
				$\nu_{14}(a_1)$ O···O stretching, Figure 8C [dilating]							
$^{66}\nu_{14}$	(361.75)	(362.00)	361.9	364.4	0.99	0.0	0.0	(0.25)	1.22	1.25	1.00
$^{88}\nu_{14}$			353.4	355.5	0.99	8.8	8.5				
$^{D}\nu_{14}$	(359.40)	(359.55)	359.5	361.2	0.99	3.2	2.4	(0.15)	0.20	3.92	3.14

[a] Units for ν_v, ω_v, DS_v, and Δ_v are cm^{-1}. [b] $\nu_{v,av} = 1/2(\nu_{v,a} + \nu_{v,b})$. The ω_v are MP2/GEN-computed[15] (harmonic) frequencies. [c] The calculated isotope shifts are $(^{66}\omega_v - {}^{iso}\omega_v)$ (ν_v/ω_v). [d] The observed spectral doublet separations are $DS_v = \nu_{v,b} - \nu_{v,a}$. For a_1 and A_1 transitions from the ground state $DS_v = |\Delta_v - \Delta_0|$ with $^{66}\Delta_0 = 0.974$ and $^{D}\Delta_0 = 0.051$ cm^{-1}. For ^{86}Tp(OH) and ^{88}Tp(OH) the ZP splitting estimates are $^{86}\Delta_0 = 0.90$ and $^{88}\Delta_0 = 0.83$ cm^{-1} (section 3.2). The Δ_v/Δ_0 ratios in column 11, plotted in Figure 18A, show the relative dilation or damping of Δ_v relative to Δ_0. The $R_v = (^{iso}\Delta_v/{}^{iso}\Delta_0)/(^{66}\Delta_v/{}^{66}\Delta_0) = (^{iso}\Delta_v/{}^{66}\Delta_v)/(^{iso}\Delta_0/{}^{66}\Delta_0)$ ratios in column 12, plotted in Figure 18B, strengthen the correlation of the observed effects.

TABLE 2: b_2 and B_2 Transitions and Tunneling Splittings of Tp Isotopomers below 800 cm^{-1}

	doublet components[a]		vibrational frequencies[b]			vib. isotope shifts[c]		tunneling effects[d]			
vib.	$\nu_{v,a}$	$\nu_{v,b}$	$\nu_{v,ave}$	ω_v	ν_v/ω_v	calc	obs	DS_v	Δ_v	Δ_v/Δ_0	R_v
				$\nu_{27}(b_2)$ OH(OD) stretching [dilating]							
$^{66}\nu_{27}$	3102[e]	3121[e]	3112[e]	3311.1	0.94	0.0	0.0	21[f]	22	23	1.00
$^{D}\nu_{27}$	2340[e]	2344.8[e]	2342[e]	2409.4	0.97	ca. 850	770	7[f]	7	137	6
				$\nu_{37}(b_2)$ ring deformation							
$^{66}\nu_{37}$			743.4[e]	754.2	0.99	0.0	0.0				
$^{88}\nu_{37}$				741.4		12.7					
$^{D}\nu_{37}$			741.4[e]	751.5	0.99	2.7	2.0				
				$\nu_{18}(a_2)+\nu_{25}(b_1)$ (B_2)							
$^{66}\nu_{18+25}$			675	664	1.02	0.0	0.0				
$^{D}\nu_{18+25}$			676	662	1.02	2.0	−1				
				$\nu_{38}(b_2)$ ring deformation							
$^{66}\nu_{38}$			547	554.5	0.99	0.0	0.0				
$^{D}\nu_{38}$			(546)	552.4	(0.99)	2.1	(1.0)				
				$\nu_{39}(b_2)$ O···O stretching, Figure 8B [dilating]							
$^{66}\nu_{39}$			348	348.7	1.0	0.0	0.0				
$^{88}\nu_{39}$			336.0	340.8	0.99	7.8	12				
$^{D}\nu_{39}$	335.71	336.15	335.93	332.7	1.01	16.1	12.	0.44[g]	0.39	7.6	
				$\nu_8(a_1) - \nu_{39}(b_2)$ hot band with Δ_{39} as lower state							
$^{D}\nu_{8-39}$	762.73	763.15						0.42[h]	0.37	7.3	

[a] −[d] See footnotes for Table 1. [e] Neon matrix isolated samples.[33] [f] Estimated DS_{27} values for the gas phase doublets.[33] [g] $DS_{39} = \Delta_{39} + \Delta_0$ for Z transition dipole component. [h] $DS_8-39 = \Delta_{39} + \Delta_8 \approx \Delta_{39} + \Delta_0$ (section 3.7).

of the singly labeled ^{18}O tropolone isotopomer. These important results, together with the vibrational state-specific splittings $^{iso}\Delta_v$ reported in the present work, emphasize the inherent multidimensional character of the tunneling mechanism for the tautomerization of Tp.

2. Procedures

As described previously,[11−14] the FTIR spectra of gaseous tropolone isotopomers were recorded at spectral resolutions reaching 0.0025 cm^{-1} using a Bruker IFS 120HR spectrophotometer. Tp sublimate at its vapor pressure near 0.01 Torr at 298 K was contained in a multipass (White) IR absorption cell set for a path length of 32 m. Tp(OD) was prepared by H/D exchange between Tp(OH) and D_2O(l), and interior surfaces of the absorption cell were repeatedly deuterated using D_2O(g). Transitions due to residual Tp(OH) and/or to isotopic water vapor have been electronically removed from most figures presented in this article. An $^{18}O,^{18}O$-tropolone(OH) sample was prepared through acid-catalyzed $^{18}O/^{16}O$ exchange between Tp(OH) dissolved in $H_2{}^{18}O$(l) as previously described.[14]

Assignments proposed for the observed anharmonic vibrations of the Tp isotopomers are primarily based on experimental data such as band profiles, isotope effects, overtone/combination transitions, etc., with valuable guidance provided by unscaled harmonic spectra computed[15,16] via quantum chemistry using the standard theoretical methods available in the Gaussian 98 codes.[28] Hardware available for our spectral computations[15,16] limited the basis (called GEN for reference) to 6-311G(df,pd) functions for the C−OH···O═C ring and 6-311G(d,p) functions for the C_5H_5 loop, with second-order Møller-Plesset (MP2)

TABLE 3: a_2 and A_2 Transitions and Tunneling Splittings of Tp Isotopomers below 800 cm^{-1}

	doublet components[a]		vibrational frequencies[b]			vib. isotope shifts[c]		tunneling effects[d]			
vib.	$\nu_{v,a}$	$\nu_{v,b}$	$\nu_{v,ave}$	ω_v	ν_v/ω_v	calc	obs	DS_v	Δ_v	Δ_v/Δ_0	R_v
				$\nu_c = \nu_{13}(a_1)+\nu_{18}(a_2)$ (A_2) [dilating]							
$^{66}\nu_c$	710.12	712.19	711.15	783.0	0.91	0.0	0.0	2.07	1.10	1.13	1.00
$^{D}\nu_c$	709.66	709.86	709.76	775.8	0.91	6.6	1.4	0.20	0.15	2.94	2.60
				$\nu_{17}(a_2)$ COD torsion/CO···OC twisting/CH wagging [dilating]							
$^{66}\nu_{17}$				642.3		0.0					
$^{D}\nu_{17}$	586.36	586.64	586.50	643.5	0.91	−1.1		0.28	0.23	4.5	
				$\nu_{18}(a_2)$ skeletal deformation							
$^{66}\nu_{18}$			271	342.1	0.79	0.0	0.0				
$^{D}\nu_{18}$			271	341.8	0.79	0.2	0.0				
				$\nu_{19}(a_2)$ OCCO twisting/skeletal deformation							
$^{66}\nu_{19}$			110	102.4	1.07	0.0	0.0				
$^{D}\nu_{19}$			109	102.4	1.06	0.0	1.0				

[a−d] See footnotes for Table 1.

TABLE 4: b_1 and B_1 Transitions and Tunneling Splittings of Tp Isotopomers below 800 cm^{-1}

	doublet components[a]		vibrational frequencies[b]			vib. isotope shifts[c]		tunneling effects[d]			
vib.	$\nu_{v,a}$	$\nu_{v,b}$	$\nu_{v,ave}$	ω_v	ν_v/ω_v	calc	obs	DS_v	Δ_v	Δ_v/Δ_0	R_v
				$\nu_c = \nu_{14}(a_1)+\nu_{25}(b_1)$ (B_1) [dilating]							
$^{66}\nu_c$	753.72	754.53	754.13	744.5	1.01	0.0	0.0	0.81	1.78	1.83	1.00
$^{86}\nu_c$	750.02	751.87	750.95	738.7	1.02	5.9	3.2	1.85	1.68[e]	1.87	1.02
$^{88}\nu_c$	749.29	750.03	749.66	733.1	1.02	11.4	4.4	0.74	1.57	1.89	1.03
$^{D}\nu_c$			751.3[f]	751.5	1.00	7.0	2.8				
				$\nu_{22}(b_1)$ COH/D torsion [damping]							
$^{66}\nu_{22}$	751.08	751.96	751.5	879.3	0.85	0.0	0.0	0.88	0.09	0.09	1.00
$^{86}\nu_{22}$	750.38	750.96	750.7	878.3	0.85	0.9	0.8	0.58	0.08[e]	0.09	1.00
$^{88}\nu_{22}$	749.63	750.38	750.0	877.3	0.85	1.7	1.5	0.75	0.08	0.10	1.11
$^{D}\nu_{22}$	(554.81)	(554.85)	554.83	636.1	0.87	ca. 212	197	(0.04)	0.01	0.20	2.2
				$\nu_{23}(b_1)$ symmetrical CH wag [dilating]							
$^{66}\nu_{23}$	716.38	716.91	716.65	744.6	0.96	0.0	0.0	0.53	1.50	1.54	1.00
$^{86}\nu_{23}$	714.69	715.36	715.03	744.3	0.96	0.3	1.6	0.67	1.45[e]	1.61	1.05
$^{88}\nu_{23}$	713.31	713.87	713.59	744.1	0.96	0.5	3.1	0.56	1.39	1.67	1.08
$^{D}\nu_{23}$	716.175	716.216	716.195	744.6	0.96	0.0	0.5	0.041	0.092	1.80	1.17
				$\nu_{25}(b_1)$ asymmetrical out-of-plane ring deformation [damping]							
$^{66}\nu_{25}$	393.10	393.75	393.43	380.1	1.03	0.0	0.0	0.65	0.32	0.33	1.00
$^{88}\nu_{25}$			391.8	377.6	1.04	2.6	1.6				
$^{D}\nu_{25}$	(390.99)	(391.01)	391.00	377.6	1.04	2.6	2.4	(0.02)	0.03	0.59	1.79
				$\nu_{26}(b_1)$ skeletal folding deformation							
$^{66}\nu_{26}$			177	167.7	1.06	0.0	0.0				
$^{D}\nu_{26}$			174	166.8	1.04	0.9	3				

[a−d] See footnotes for Table 1. [e] $^{86}\Delta_v = 1/2(^{66}\Delta_v + ^{88}\Delta_v)$. [f] Neon matrix isolated sample.

theory used to approximate the electron correlation energy. MP2/GEN level computations of general anharmonic effects were not feasible here and would be expected to add little to the reliability of the vibrational assignments. Burns, Murdock, and Vaccaro[29] computed harmonic spectra for Tp at the DFT-(B3LYP)/aug-cc-pVDZ, MP2/aug-cc-pVDZ, and CCSD/aug-cc-pVDZ levels of theory. In the 350−800 cm^{-1} range the three methods produce computed fundamentals ω_v which agree to about 1−3% for in-plane and 3−8% for out-of-plane modes. The MP2/GEN computations fall within or near these ranges for ω_v. Other recent computations of the monomer vibrations are by Rostkowska et al.,[30] while vibrations concerned with H bond dynamics of the Tp_2 dimer were treated by Wójcik, Boczar, and Stoma.[25]

The states of nonrigid Tp are classified according to the G_4 molecular symmetry group using notation of the isomorphous C_{2v} point group. For Tp(OH) the fundamental vibration frequencies and their indices descend in each symmetry block with $\nu_1-\nu_{14}$ in a_1, $\nu_{15}-\nu_{19}$ in b_1, $\nu_{20}-\nu_{26}$ in a_2, and $\nu_{27}-\nu_{39}$ in b_2. The minimum energy configuration of Tp has C_2 point group symmetry. Then each of its computed normal modes has hybrid vibrational character comprised of longitudinal (Z, a_1) and transverse (Y, b_2) transition dipole components for in-plane modes, and out-of-plane (X, b_1) and (zero, a_2) transition dipole components for out-of-plane modes. The observed fundamentals are labeled according to which hybrid component is the most intense.

3. Observed Results and Discussion

3.1. $\nu_{22}(b_1)$ (COH Torsion) and $\nu_{14}(a_1) + \nu_{25}(b_1)$ (B_1). These two vibrations demonstrate the general spectral behaviors seen for many FTIR transitions of Tp. In Figure 2A, an overview is shown for the sharp Q branch doublets observed[11,12,14] for ν_{22}-(b_1) of Tp(OH). The fundamental is accompanied by a room-temperature hot band progression $\nu_{22} + N\nu_{19} - N\nu_{19}$ [Type C rotational profiles; $N = 1-7$ with $\nu_{19}(a_2) = 110$ cm^{-1} (OCCO twisting/skeletal deformation)]. The $\nu_{22}(b_1)$ doublet transitions for the ^{iso}Tp(OH) oxygen isotopomers are shown in Figure 3 with the proposed origins for the components placed toward the blue edge of each absorbance profile. In this work the doublet for $^{88}\nu_{22}(b_1)$ is blue-shifted about 0.2 cm^{-1} from the previously proposed origins[14] which were obtained by considering the absorbance in Figure 3C as due to one, rather than two,

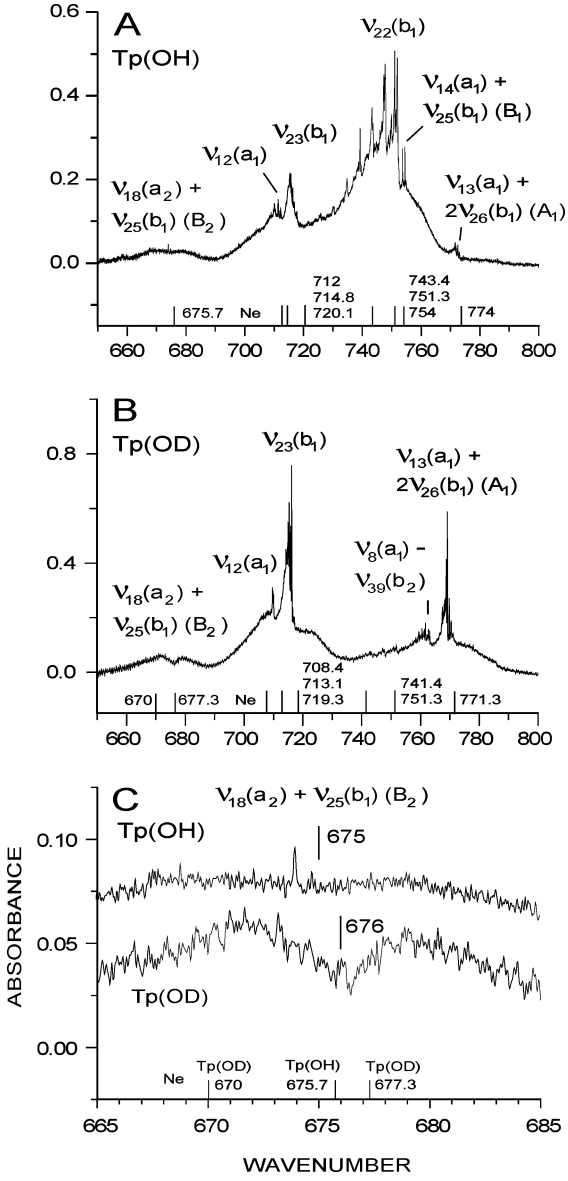

Figure 2. FTIR absorption spectra of gaseous Tp(OH) and Tp(OD). Transition origins for Ne matrix-isolated samples[15,31] at ca. 5 K are shown along the abscissa.

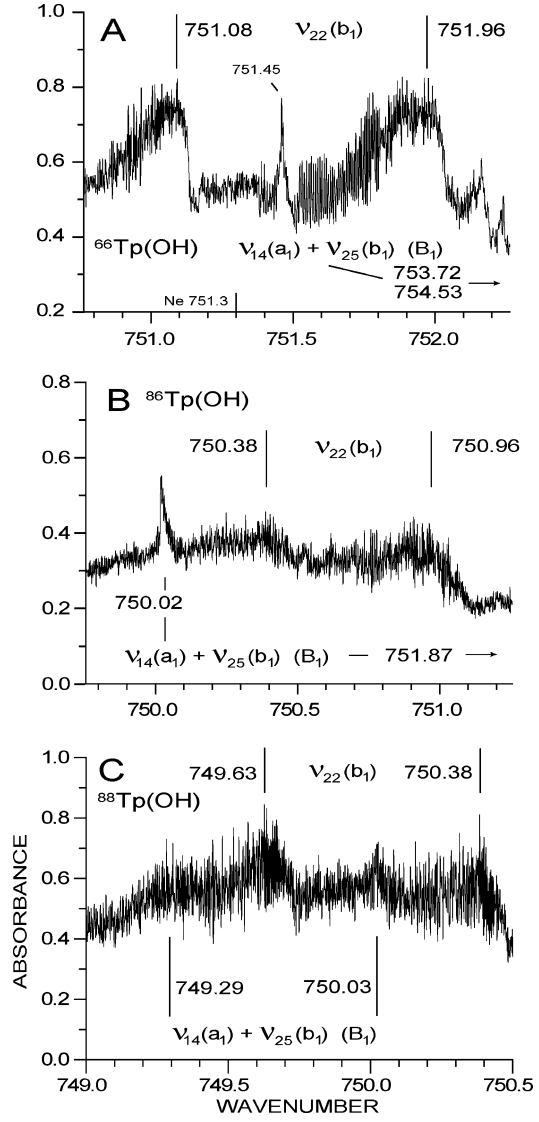

Figure 3. Spectral doublets for $\nu_{22}(b_1)$ (OH torsion) and $\nu_{14}(a_1) + \nu_{25}(b_1)$ (B_1) of the ^{iso}Tp(OH) oxygen isotopomers. The 750.02 cm^{-1} peak of ^{86}Tp(OH) in (B) contributes to the 750.03 cm^{-1} absorbance in (C).

spectral doublets. Components of the $^{66}\nu_{22}(b_1)$ spectral doublet (see Table 4) have the separation $^{66}DS_{22} = |^{66}\Delta_{22} - ^{66}\Delta_0| = 0.88\ cm^{-1}$. This yields, with $^{66}\Delta_0 = 0.974\ cm^{-1}$, the damped splitting estimate $^{66}\Delta_{22} = 0.09\ cm^{-1} = 0.09\ ^{66}\Delta_0$ for the COH torsion state. As seen below the alternative dilated splitting $^{66}\Delta_{22} = 1.85\ cm^{-1} = 1.90\ ^{66}\Delta_0$ is inordinately large for $\nu_{22}(b_1)$ and is thus rejected. For ^{88}Tp(OH) the spectral doublet separation is $^{88}DS_{22} = |^{88}\Delta_{22} - ^{88}\Delta_0| = 0.75\ cm^{-1}$. Using $^{88}\Delta_0 = 0.83\ cm^{-1}$, as estimated in section 3.2, produces $^{88}\Delta_{22} = 0.08\ cm^{-1} = 0.10\ ^{88}\Delta_0$; parallel results for $^{86}\Delta_{22}$ and for $^{D}\Delta_{22}$ (Sect. 3.3) are included in Table 4.

The FTIR measurement of fundamentals in the 300−400 cm^{-1} range bears on the interpretation of absorbances seen in Figure 2A at 754 cm^{-1} for Ne-isolated ^{66}Tp(OH) and at 753.724, 754.525 cm^{-1} for gaseous[11,12,14] ^{66}Tp(OH). Previously attributed to transitions supporting a ca. 10 cm^{-1} contortional tunneling splitting,[11−16] they are now reassigned as the $\nu_{14}(a_1) + \nu_{25}(b_1)$ (B_1) combination mode doublet. This is calculated as 361.9 + 393.4 = 755.3 cm^{-1} using averages of the observed gas phase doublet frequencies. The data for gaseous ^{66,86,88}Tp(OH) appear in Figure 3 and Table 4. The $\nu_{14}(a_1) + \nu_{25}(b_1)$ absorbances are probably intensified through anharmonic couplings to the adjacent intense $\nu_{22}(b_1)$ COH torsion fundamentals. The $^{66}DS_{14+25} = |^{66}\Delta_{14+25} - 0.974| = 0.81\ cm^{-1}$ value for ^{66}Tp(OH) produces the dilated splitting $^{66}\Delta_{14+25} = 1.78\ cm^{-1} = 1.83\ ^{66}\Delta_0$, with the dilation anticipated from its $\nu_{14}(a_1)$ (O···O stretching) constituent. The $^{iso}\Delta_{14+25}$ splittings yield $^{iso}\Delta_v/^{iso}\Delta_0$ ratios (col. 11 in Table 4) that obey the inequalities $^{66}\Delta_v/^{66}\Delta_0 < ^{86}\Delta_v/^{86}\Delta_0 < ^{88}\Delta_v/^{88}\Delta_0$ and $^{H}\Delta_v/^{H}\Delta_0 < ^{D}\Delta_v/^{D}\Delta_0$ holding for all oxygen and hydrogen isotopomers, respectively, for which data are available. The $\nu_{14}(a_1) + \nu_{25}(b_1)$ (B_1) transition of Tp(OD) is far removed from, and not intensified by, $^{D}\nu_{22}(b_1) = 554.83\ cm^{-1}$ and it is not observed in the gas-phase data. The calculated estimate, 359.5 + 391.0 = 750.5 cm^{-1}, falls near a weak peak found in Ne-isolated Tp(OD) at 751.3 cm^{-1}. However, this peak is certainly due in part to absorbance by Tp(OH) impurity.

3.2. Estimate for $^{88}\Delta_0$. Since $^{88}\Delta_0$ has not yet been determined by microwave spectroscopy, a value is estimated here by correlating the $^{88}\Delta_v/^{66}\Delta_v$ tunneling splitting ratios obtained for four vibrational transitions. As shown above $\nu_{22}(b_1)$ is a damping vibration yielding $^{66}\Delta_{22} < ^{66}\Delta_0$, while $\nu_{14}(a_1) + \nu_{25}(b_1)$ (B_1) is dilating with $^{66}\Delta_{14+25} > ^{66}\Delta_0$. The other two vibrations, $\nu_{13}(a_1)$ and $\nu_{23}(b_1)$, are also dilating modes (vida infra). The relation $^{66}DS_v = |^{66}\Delta_v - ^{66}\Delta_0|$ with $^{66}\Delta_0 = 0.974$

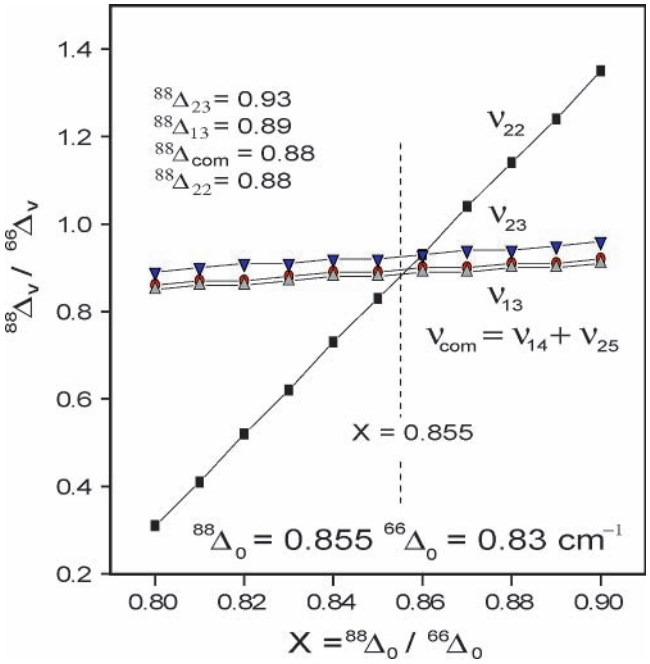

Figure 4. Plot determining $^{88}\Delta_0 = 0.83$ cm^{-1} by estimating $X = {}^{88}\Delta_0/{}^{66}\Delta_0 = 0.855$ (cf. section 3.2).

cm^{-1} for each vibration of ^{66}Tp(OH) is paralled by $^{88}DS_v = |^{88}\Delta_v - {}^{88}\Delta_0| = |^{88}\Delta_v - X^{66}\Delta_0|$ for each vibration of ^{18}O,^{18}O-Tp(OH). It is desired to choose a best value for the parameter $X = {}^{88}\Delta_0/{}^{66}\Delta_0$. The observed $^{88}DS_v$ values produce $^{88}\Delta_0$ and $^{88}\Delta_v$ values for each trial X. The resulting vibrational state-specific $^{88}\Delta_v/{}^{66}\Delta_v$ ratios are plotted in Figure 4 as a function of X. For the five $^{88}\Delta_v/{}^{66}\Delta_v$ ratios the average deviation from the mean takes its minimum value at $X = 0.855$. Thus, the assumed criterion that the $^{88}\Delta_v/{}^{66}\Delta_v$ ratios should be as nearly as possible independent of vibrational state yields $^{88}\Delta_0 = 0.855$ $^{66}\Delta_0 = 0.83$ cm^{-1}. This value is entered in col. 2 of Table 5 and is used to determine the $^{88}\Delta_v$ splittings entered in Tables 1 and 4. The estimate $^{86}\Delta_0 = 1/2(0.974 + 0.83) = 0.90$ cm^{-1} is entered in column 3 of Table 5 for ^{86}Tp(OH). The available isotopic splittings and splitting ratios are discussed in greater detail in section 4.

3.3. $\nu_{22}(b_1)$ (COD Torsion). The $\nu_{22}(b_1)$ absorbance profiles shown in Figures 2A for Tp(OH) and 5A for Tp(OD) show a superficial similarity, while Figure 5B shows the unresolved Q branch doublets observed for $^{D}\nu_{22}(b_1)$ and its first two hot bands. The ca. 0.35 cm^{-1} full width at half-maximum (fwhm) values for the Tp(OD) profiles are near those observed for the resolved doublet components of $\nu_{22}(b_1)$ for Tp(OH). The ratio $^{H}\Delta_{22}/{}^{H}\Delta_0 = 0.09$ observed for Tp(OH) suggests the analogous damping $^{D}\Delta_{22} < {}^{D}\Delta_0$. The weak beat pattern and probable doublet maxima seen in Figure 5C for $^{D}\nu_{22}(b_1)$ insinuate a narrow doublet character. The proposed doublet origins yield $^{D}DS_{22} = 0.04$ cm^{-1} $= |^{D}\Delta_{22} - 0.051|$ to give $^{D}\Delta_{22} = 0.01$ cm^{-1} $= 0.20$ $^{D}\Delta_0$ as entered in Table 4. These results for $\nu_{22}(b_1)$ fit the pattern $^{H}\Delta_v/{}^{H}\Delta_0 < {}^{D}\Delta_v/{}^{D}\Delta_0$ that is observed throughout Tables 1−4.

3.4. $\nu_{17}(a_2)$ (COD Torsion/CO···OC Twisting/CH Wagging). Figure 5A shows the adjacent out-of-plane $^{D}\nu_{17}(a_2)$ and $^{D}\nu_{22}(b_1)$ transitions, with detail for the central Q spikes for $^{D}\nu_{17}(a_2)$ and its hot bands shown in Figure 6A. The prominent absorbances show the strong hybrid character (nonzero X transition dipole component) of $\nu_{17}(a_2)$ and the probable presence of absorbance-enhancing nonharmonic interactions between $\nu_{17}(a_2)$ to $\nu_{22}(b_1)$. Separations for the X-polarized doublet components are $DS_{17} = \Delta_{17} + \Delta_0$ and $DS_{22} = |\Delta_{22} - \Delta_0|$. The inset in Figure 6A clearly shows the 586.64 cm^{-1} spike profile is too narrow to host a spectral doublet with $DS_v = \Delta_v + \Delta_0$, and the two most intense transitions are therefore attributed to the $^{D}\nu_{17}(a_2)$ doublet. Then $^{D}DS_{17} = 0.28 = {}^{D}\Delta_{17} + 0.051$ cm^{-1} to give $^{D}\Delta_{17} = 0.23$ cm^{-1} $= 4.5$ $^{D}\Delta_0$ as listed in Table 3. This result ranks $^{D}\Delta_{17}$ (as coupled to $^{D}\Delta_{22}$) close to the nominal O···O stretches (sections 3.6−3.8) as a promoter of the tautomerization process in Tp(OD).

TABLE 5: Tunneling Parameters for Tp(OH) Isotopomers in the ZP States

	$^{as}\Delta_0{}^2 = \Delta_0{}^2 + \delta_0{}^2$					
isotopomer	$^{as}\Delta_0$ obs.[a]	Δ_0 trial[b]	% damping rel. to 0.974[c]	δ_0 calc.[d]	ΔZPE[e]	δ_0/ΔZPE
Tp(OH)	0.974	0.974	0.0•	0	0	
$^{13}C_5$	0.970	0.970	0.4•	0	0	0
$^{13}C_{4(6)}$	0.980	0.964	1.0•	0.17	−0.91	0.19
		0.955	2.0	0.22	−0.91	0.24
		0.925	5.0	0.32		0.35
$^{13}C_{3(7)}$	1.130	0.954	2.0	0.61	−1.58	0.39
		0.944	3.0	0.62		0.39
	1.130	0.935	4.0•	0.63	−1.58	0.40
		0.925	5.0	0.65		0.41
$^{18}O_{8(9)}$	1.70	0.90	7.6•	1.44	−2.59	0.56
$^{18}O_8$,$^{18}O_9$	0.83	0.83	14.8•	0	0	0
$^{13}C_{2(1)}$	0.895	0.974	0.0	0.38i	+1.39	
		0.895	9.2	0.00		
		0.877	10.0	0.18		0.13
	0.895	0.857	12.0•	0.26	+1.39	0.19
		0.827	15.0	0.34		0.24

[a] $^{as}\Delta_0$ is the observed ZP tunneling splitting in cm^{-1}. Values for the ^{13}C isotopomers, for $^{18}O_{8(9)}$ [^{86}Tp(OH)], and for $^{18}O_8$,$^{18}O_9$ [^{88}Tp(OH)] are from ref 9, ref 50, and Figure 4, respectively. [b] Δ_0 is the tunneling splitting in cm^{-1} for the equal double minimum PES obtained when $\delta_0 = 0$. [c] Percent damping of the isotopomer Δ_0 value relative to $\Delta_0 = 0.974$ cm^{-1} for Tp(OH). A plausible correlation of damping values for the seven ZP states is highlighted by •. [d] δ_0 is the energy offset between minima of the double minimum PES in cm^{-1} as calculated from $^{as}\Delta_0{}^2 = \Delta_0{}^2 + \delta_0{}^2$. [e] ΔZPE is the theoretically estimated difference[9] between the ZP energies of the tautomers.

The MP2/GEN-computed normal modes shown in Figure 7 for the $\nu_{22}(b_1)$ and $\nu_{17}(a_2)$ tautomer and saddle-point (SP) configurations of Tp(OD) bear on explaining the observed behavior. Q_{22} and Q_{17} suggest in-phase and out-of-phase oscillations between COD torsion and a complex of small internal coordinate displacements, with the COD torsional amplitude much larger in $\nu_{22}(b_1)$ than in $\nu_{17}(a_2)$. The result $\omega_{22}(b_1)^{SP} > \omega_{22}(b_1)$ suggests a damping effect on $^{D}\Delta_{22}$ due to the addition of substantial vibrational energy to the SP maximum in the $^{D}\nu_{22}(b_1)$ state. With $\omega_{17}(a_2)^{SP} \approx \omega_{17}(a_2)$ this damping drive is absent in $^{D}\Delta_{17}$. Instead of damping, Q_{17} suggests the dilation of $^{D}\Delta_{17}(a_2)$ through a strong CO···OC twisting motion enhancing O···O displacement and also lengthening the CO bond distances. Finally, both Q_{22} and $Q_{22}{}^{SP}$ show large COD displacement maxima, but the COD displacement in $Q_{17}{}^{SP}$ is zero to suggest the OD···O → O···DO process is dynamically simpler in the $\nu_{17}(a_2)$ state than in the $\nu_{22}(b_1)$ state. The harmonic vibrational computations thus anticipate the observed damping of $^{D}\Delta_{22}$ and dilation of $^{D}\Delta_{17}$. They also predict that $^{H}\nu_{17}(a_2)$ has low COH torsional amplitude, a very weak IR absorbance, and a blue deuterium isotope shift of ca. 1 cm^{-1}. This supports the present lack of evidence for $\nu_{17}(a_2)$ in the FTIR spectrum of Tp(OH). The $^{H}\nu_{17}(a_2)$ and $^{H}\nu_{22}(b_1)$ fundamentals are certainly separated by more than 150 cm^{-1} [instead of 32 cm^{-1} as observed for Tp(OD)] to suggest the absence of the anharmonic/dynamic activity enhancing the $^{D}\nu_{17}(a_2)$ absorbance.

3.5. $\nu_{38}(b_2)$ (Asymmetric Ring Deformation). Figure 6B shows an isolated weak type B profile of gaseous Tp(OH) that

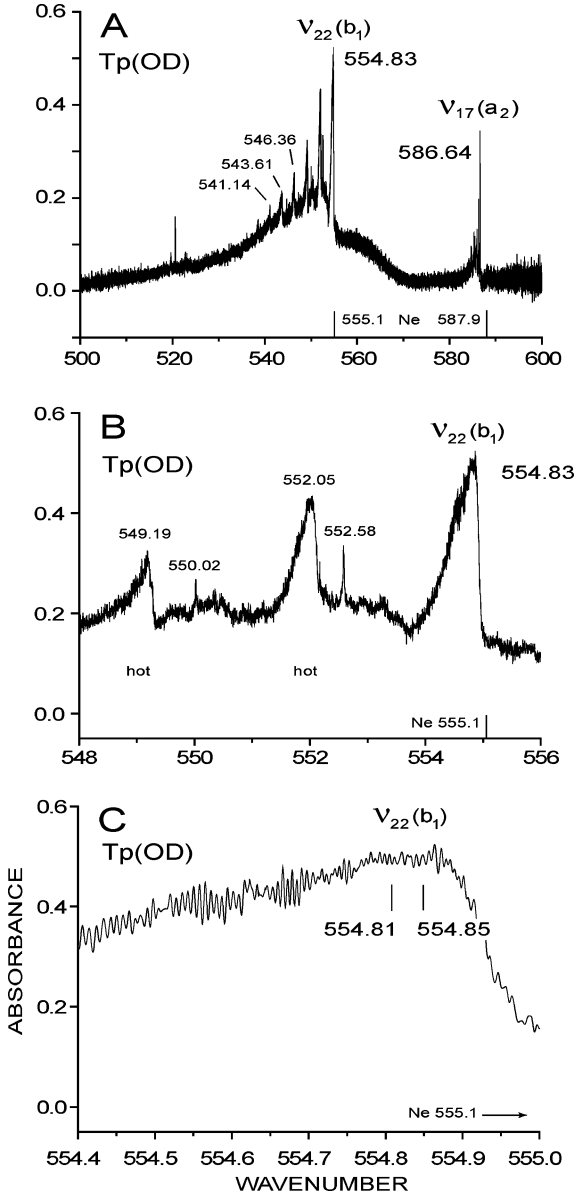

Figure 5. Views of the COD torsional fundamental $\nu_{22}(b_1)$ with close-up view (C) showing evidence for a narrow spectral tunneling doublet.

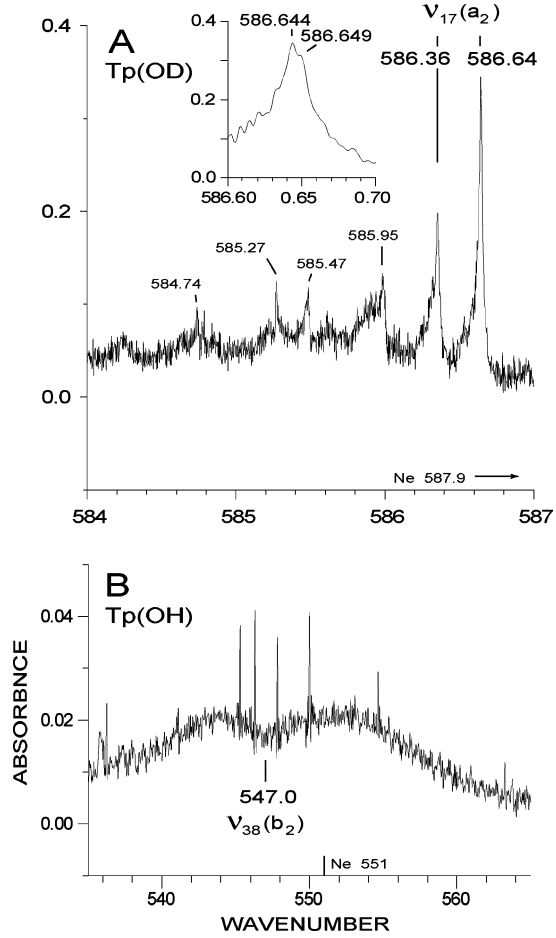

Figure 6. (A) Spectral tunneling doublet spikes for $\nu_{17}(a_2)$ of Tp(OD). (B) The weak $\nu_{38}(b_2)$ absorption of Tp(OH) with unresolved tunneling doubling. The sharp peaks are due to water lines left intentionally uncompensated for this figure.

is assigned as $\nu_{38}(b_2) = 547$ cm^{-1}. It appears at 551 cm^{-1} for Ne-isolated Tp(OH).[15,31] Its MP2/GEN-computed[15] deuterium isotope shift is 2.1 cm^{-1}, but any absorbance due to $^{D}\nu_{38}(b_2)$ is lost among the intense Tp(OD) transitions seen in Figure 5A. For Ne-isolated Tp(OD) $\nu_{22}(b_1)$ appears at 555.1 cm^{-1} with a shoulder at 551.7 cm^{-1} that may be due to $^{D}\nu_{38}(b_2)$. The gas-phase value $^{D}\nu_{38}(b_2) = 546$ cm^{-1} is entered in Table 2 as a plausible provisional estimate.

3.6. $\nu_{13}(a_1)$ (O···O Stretching, Figure 8A). Figure 9 shows the adjacent $\nu_{13}(a_1)$, $\nu_{39}(b_2)$, and $\nu_{14}(a_1)$ fundamentals and their MP2/GEN-computed normal coordinates appear in Figure 8. These three fundamentals carry the largest O···O stretching displacements computed for Tp. The central Q branch region for $\nu_{13}(a_1)$ and the red-shifted hot band doublets $\nu_{13} + N\nu_{19} - N\nu_{19}$ are shown in Figure 10A. The type A profiles yield $^{H}DS_{13} = 0.74$ cm^{-1} $= |^{H}\Delta_{13} - 0.974|$ to give $^{H}\Delta_{13} = 1.71$ cm^{-1} $= 1.76\ ^{H}\Delta_0$ as entered in Table 1, along with parallel results observed for ^{88}Tp(OH). The 1.71 value is near the $^{H}\Delta_{13}/^{H}\Delta_0 = 33/19.9 = 1.66$ ratio obtained[3,5] for the $S_1(\pi^*-\pi)$ electronic excited state. Figure 10B shows the sharper peaks observed for $^{D}\nu_{13}(a_1)$, and the doublets observed for the fundamental and first two hot bands are isolated in Figure 11, panels A and B, respectively. As already noted for $^{D}\nu_{17}(a_2)$, structured doublet components with different absorbance strengths also occur for $^{D}\nu_{13}(a_1)$. The peak maxima yield $^{D}DS_{13} = |^{D}\Delta_{13} - 0.051| = 0.27$ cm^{-1} to give $^{D}\Delta_{13} = 0.032$ cm^{-1} $= 6.3\ ^{D}\Delta_0$. The large OH/D isotope effect on the Δ_{13}/Δ_0 ratio is discussed below. The leading hot band doublets are red-shifted from $^{iso}\nu_{13}(a_1)$

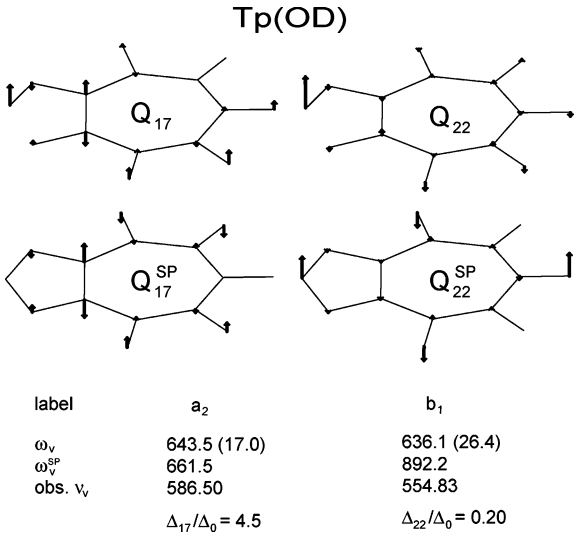

Figure 7. MP2/GEN-computed[15] (harmonic) normal coordinates for the Tp(OD) tautomer and SP configurations. The Δ_v/Δ_0 splitting ratios are observed values. Units of the parenthesized IR intensities are Å^{-1}.

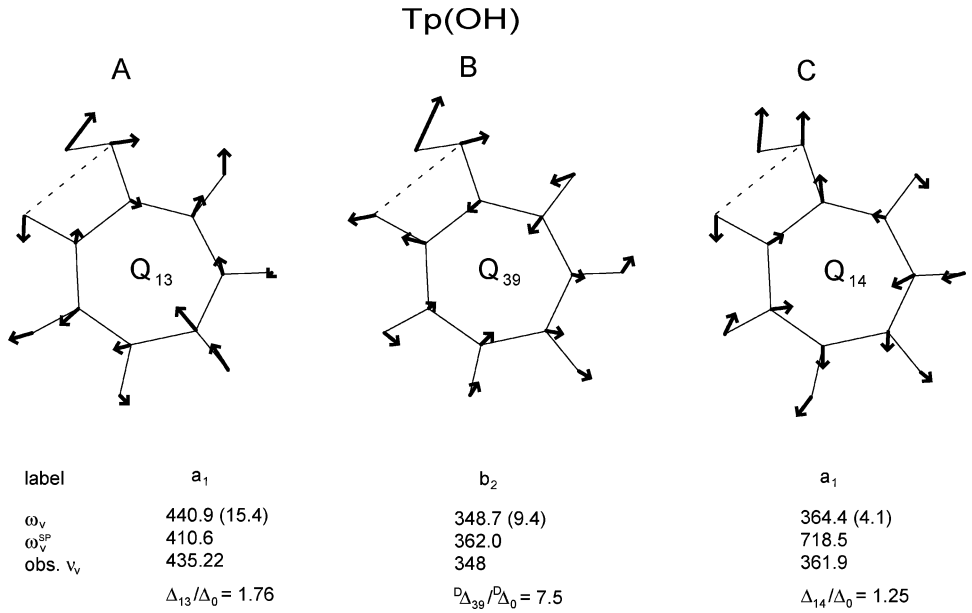

Figure 8. MP2/GEN-computed[15] (harmonic) normal coordinates for modes of Tp(OH) showing strong O···O stretching character. The Δ_v/Δ_0 splitting ratios are observed values. Units of the parenthesized IR intensities are $Å^{-1}$.

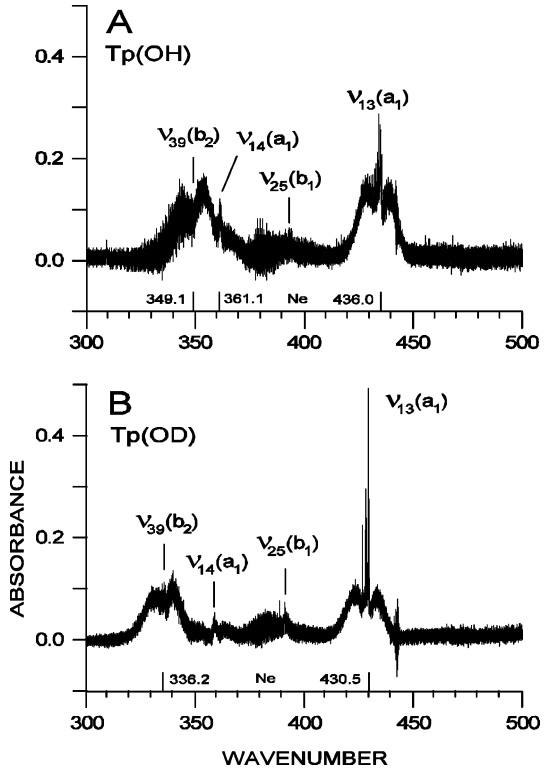

Figure 9. FTIR absorption of gaseous Tp(OH) and Tp(OD) in the 300−500 cm^{-1} region.

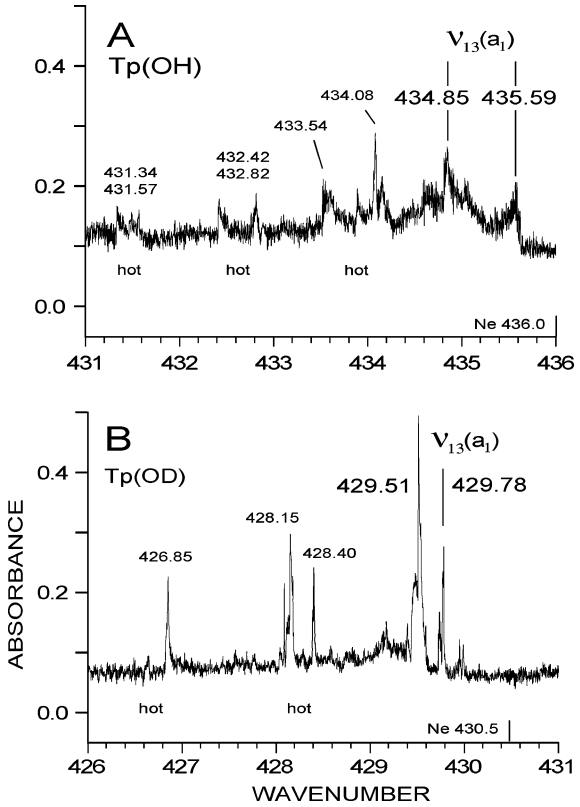

Figure 10. $\nu_{13}(a_1)$ (nominal O···O stretching) Q spike absorptions of Tp[OH(OD)].

by −1.41 cm^{-1} for Tp(OH) and −1.37 cm^{-1} for Tp(OD). The $^{iso}DS_{hot}$ = 0.54 and 0.25 cm^{-1} values are reduced from the $^{iso}DS_{13}$ values by damping effects arising with the $N\nu_{19}(a_2)$ state excitations.[11]

3.7. $\nu_{39}(b_2)$ (O···O Stretching, Figure 8B). The expected primary Y polarized transition dipole component of $\nu_{39}(b_2)$ produces the type B contours seen near 350 cm^{-1} in Figure 9, panels A and B. Since many hybrid Y−Z polarized transition dipoles are observed[13] among the Tp fundamentals, evidence for type A (Z polarized) spikes with $^{H}DS_{39} = \Delta_{39} + \Delta_0$ reaching near 3 cm^{-1} are therefore sought in the $^{H}\nu_{39}(b_2)$ region. They do not appear in Figure 12A [or in the quite similar spectrum observed for ^{88}Tp(OH)]. Figure 12B shows a marginal doublet for Tp(OD) with $^{D}DS_{39} = {}^{D}\Delta_{39} + {}^{D}\Delta_0 = 0.44$ cm^{-1}, yielding $^{D}\Delta_{39} = 0.39 = 7.6\ {}^{D}\Delta_0$. This result is equivocal but it receives support from the $\nu_8(a_1) - \nu_{39}(b_2) + N\nu_{19}(a_2) - N\nu_{19}(a_2)$ hot band progression seen near 763 cm^{-1} in Figures 2B and 12C. The primary hot band doublet is assigned as $\nu_8(a_1) - \nu_{39}(b_2)$ where $\nu_8(a_1)$ is the intense nominal COD bending fundamental.[15] Observed frequencies predict the hot band at 1103.3 − 335.93 = 767.4 cm^{-1}. The weak type A spikes are separated with $^{D}DS_{8-39} = {}^{D}\Delta_8 + {}^{D}\Delta_{39}$. For Tp(OH) the $^{H}\Delta_8$ splitting is within[13] 10% of $^{H}\Delta_0$ to suggest $^{D}\Delta_8 \approx {}^{D}\Delta_0 = 0.051$ cm^{-1} as a reasonable

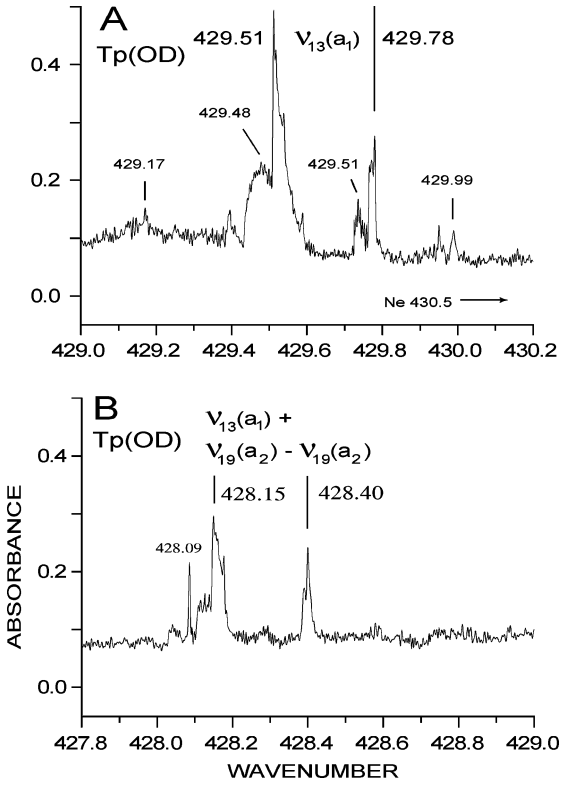

Figure 11. (A) Q branch details for $\nu_{13}(a_1)$ of Tp(OD). (B) The leading hot band for $\nu_{13}(a_1)$.

approximation for Tp(OD). Then, as entered in Table 2, ${}^{D}DS_{8-39} = (0.05 + {}^{D}\Delta_{39}) = 0.42\ cm^{-1}$ to give ${}^{D}\Delta_{39} = 0.37\ cm^{-1} = 7.3\ {}^{D}\Delta_0$ (versus $7.6\ {}^{D}\Delta_0$ obtained above).

3.8. $\nu_{14}(a_1)$ (O···O Stretching, Figure 8C). The type A absorption spikes for $\nu_{14}(a_1)$ appear near 360 cm^{-1} in Figure 9, panels A and B. They are expanded in Figure 13, panels A and B, where much of the absorbance region is attributable to the $\nu_{14}(a_1) + \nu_{19}(a_2) - \nu_{19}(a_2)$ hot band doublet. The vague $\nu_{14}(a_1)$ doublet structures gain significance by yielding results that parallel those already observed for $\nu_{13}(a_1)$ and $\nu_{39}(b_2)$. Tentative doublets origins selected for $\nu_{14}(a_1)$ and shown in Figure 13 have ${}^{H}DS_{14} = 0.25\ cm^{-1}$ and ${}^{D}DS_{14} = 0.15\ cm^{-1}$. These give ${}^{H}\Delta_{14} = 1.22\ cm^{-1} = 1.25\ {}^{H}\Delta_0$, and ${}^{D}\Delta_{14} = 0.20\ cm^{-1} = 3.9\ {}^{D}\Delta_0$, as entered into Table 1. The ${}^{H,D}\Delta_{14}$ values are damped relative to ${}^{H,D}\Delta_{13}$ and ${}^{D}\Delta_{39}$. The MP2/GEN-computed data in Figure 8 shows ${\omega_{14}}^{SP} - {\omega_{14}}^{taut} = 718.5-364.4\ cm^{-1}$ to suggest damping through a large vibrational energy contribution to the $\nu_{14}(a_1)$ state PES SP barrier. Analogous damping drives are absent for SPs of the $\nu_{13}(a_1)$ and $\nu_{39}(b_2)$ states.

3.9. $\nu_{25}(b_1)$ (Asymmetrical Out-of-Plane Ring Deformation). The weak absorbance spikes in the 375−400 cm^{-1} regions of Figure 9, panels A and B, correspond to the MP2/GEN-computed out-of-plane fundamentals[15] ${}^{H}\omega_{25}(b_1) = 380.1$ and ${}^{D}\omega_{25}(b_1) = 377.6\ cm^{-1}$. Figure 14A shows the type C spikes for ${}^{H}\nu_{25}(b_1)$. These produce ${}^{H}DS_{25} = 0.65\ cm^{-1} = |{}^{H}\Delta_{25} - {}^{H}\Delta_0|$ to give either the large dilated splitting ${}^{H}\Delta_{25} = 1.62 = 1.66\ {}^{H}\Delta_0$ or the damped splitting ${}^{H}\Delta_{25} = 0.32\ cm^{-1} = 0.33\ {}^{H}\Delta_0$. The damped parameters fit the correlation of ${}^{iso}\Delta_{\nu}/{}^{iso}\Delta_0$ ratios first noted in section 3.1 and they are entered into Table 4. Figure 14B shows the narrow doublet for ${}^{D}\nu_{25}(b_1)$ at 391.00 cm^{-1}. This is given the estimate ${}^{D}DS_{25} = |{}^{D}\Delta_{25} - 0.051| = 0.02\ cm^{-1}$ to produce ${}^{D}\Delta_{25} = 0.03\ cm^{-1} = 0.59\ {}^{D}\Delta_0$. The peaks at 390.89, 391.22 cm^{-1} for Tp(OH) and at 388.60 cm^{-1} for Tp(OD) are attributed to the leading hot bands in $\nu_{19}(a_2)$ red-shifted by −2.37 and −2.40 cm^{-1}, respectively.

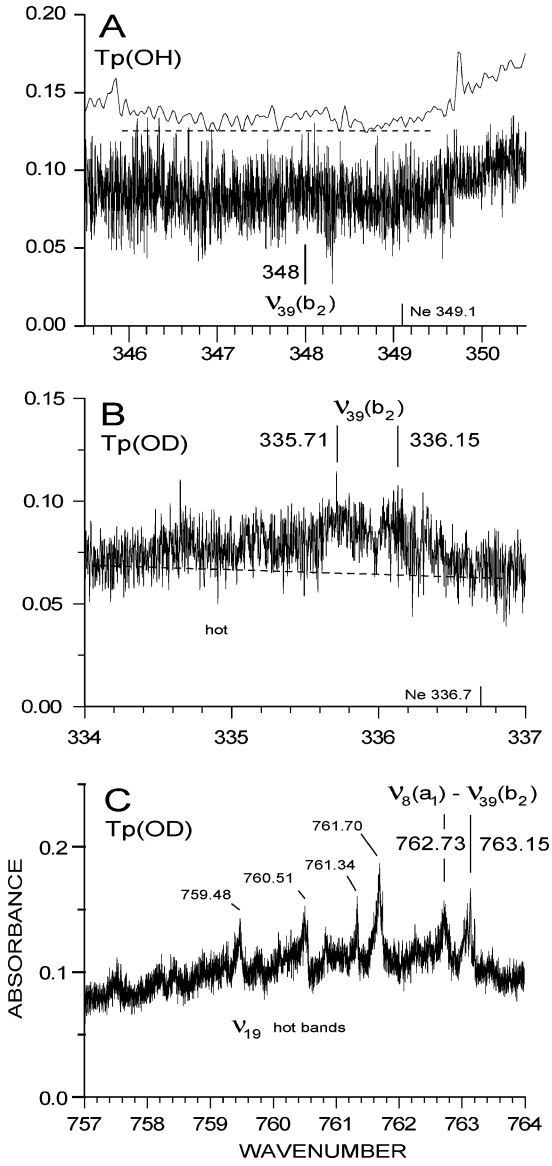

Figure 12. (A) Unresolved type B profiles of ${}^{H}\nu_{39}(b_2)$. (B) Marginal doublet with type A (Z polarized) hybrid components and ${}^{D}DS_{39} = {}^{D}\Delta_{39} + {}^{D}\Delta_0$. (C) Spectral doublet for the $\nu_8(a_1)-\nu_{39}(b_2)$ hot band transition of Tp(OD) with ${}^{D}DS_{8-39} \approx {}^{D}\Delta_{39} + {}^{D}\Delta_0$ (section 3.7).

3.10. $\nu_{26}(b_1)$, $\nu_{18}(a_2)$, and $\nu_{19}(a_2)$. According to single level dispersed fluorescence data[5,32] the three lowest frequency fundamentals of Tp(OH)[Tp(OD)] are: $\nu_{18}(a_2)$ (skeletal deformation) = 271[271] cm^{-1}; $\nu_{26}(b_1)$ (CO skeletal folding deformation) = 177[174] cm^{-1}; and $\nu_{19}(a_2)$ (OCCO twist/skeletal distortion) = 110[109] cm^{-1}. No evidence for the very weak[15,29] $\nu_{18}(a_2)$ and $\nu_{26}(b_1)$ fundamentals appeared in FTIR scans reaching down to 150 cm^{-1}.

3.11. $\nu_{18}(a_2) + \nu_{25}(b_1)$ (B_2). The spectral overviews in Figure 2, panels A and B, each show a weak IR absorbance near 675 cm^{-1} with an apparent type B rotational profile indicating a b_2 or B_2 upper state. The observations $\nu_{25}(b_1) = 393.43\ cm^{-1}$ for Tp(OH) and 391.00 cm^{-1} for Tp(OD) allow the 675 cm^{-1} transitions to be reassigned as $\nu_{18}(a_2) + \nu_{25}(b_1)$ (B_2) instead of as an a_1 fundamental. The transitions are calculated from observed frequencies as 271 + 393.43 = 664 cm^{-1} for Tp-(OH) and 271 + 391.00 = 662 cm^{-1} for Tp(OD). The distorted Type B profiles in Figure 2C [and also for the ^{88}Tp(OH) absorption profile] and the two peaks observed for Ne-isolated Tp(OD) indicate at least two transitions contribute to each observed profile.

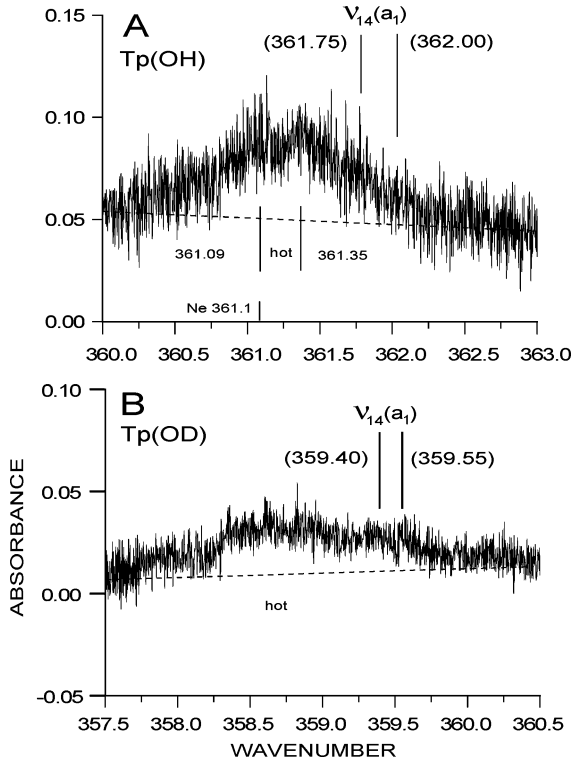

Figure 13. Proposed doublets for $\nu_{14}(a_1)$ and hot bands of Tp[OH-(OD)].

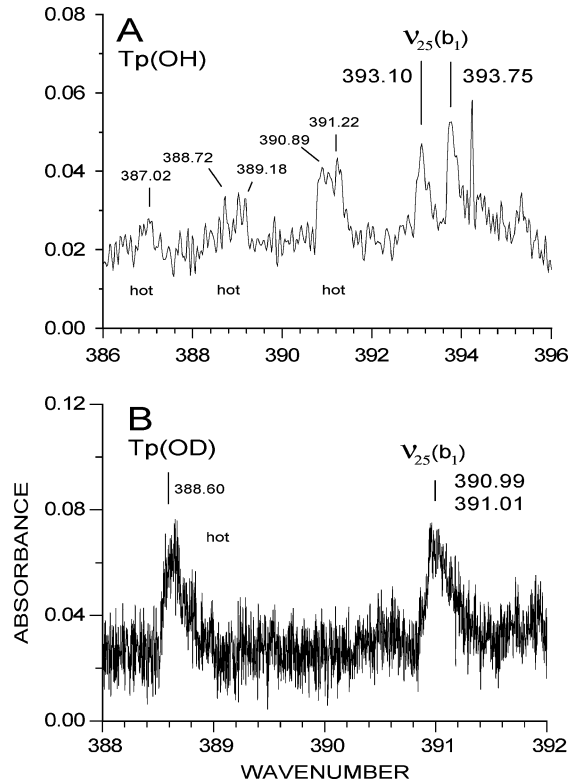

Figure 14. (A) Resolved doublet for ${}^{H}\nu_{25}(b_1)$. (B) Unresolved doublet for ${}^{D}\nu_{25}(b_1)$.

3.12. $\nu_{23}(b_1)$ (Symmetrical CH Wagging). Figure 2, panels A and B, show absorbance spikes near 717 cm^{-1} attributed to $\nu_{23}(b_1)$. Figure 15D shows the very sharp Q spike doublet for ${}^{D}\nu_{23}(b_1)$ producing ${}^{D}DS_{23} = 0.041 = |{}^{D}\Delta_{23} - 0.051|$ cm^{-1}. Then ${}^{D}\Delta_{23} = 0.092$ $cm^{-1} = 1.80$ ${}^{D}\Delta_0$ as entered in Table 4. The damped splitting value ${}^{D}\Delta_{23} = 0.010$ $cm^{-1} = 0.20$ ${}^{D}\Delta_0$ is rejected because it does not follow the correlation of ${}^{iso}\Delta_v/{}^{iso}\Delta_0$ ratios. The central absorption spike regions for ^{66,68,88}Tp(OH), reassigned from the proposals of ref 14, are shown in Figure 15, panels A−C, respectively.[14] The dilated splitting parameters are listed in Table 4 and the resulting splitting ratios were used in section 3.2 to help estimate the ZP splitting ${}^{88}\Delta_0 = 0.83$ cm^{-1}. The $\nu_{23}(b_1)$ doublets have both red-shifted hot bands $\nu_{23}(b_1) + N\nu_{19}(a_2) - N\nu_{19}(a_2)$ and blue-shifted hot bands $\nu_{23}(b_1) + N\nu_{26}(b_1) - N\nu_{26}(b_1)$.

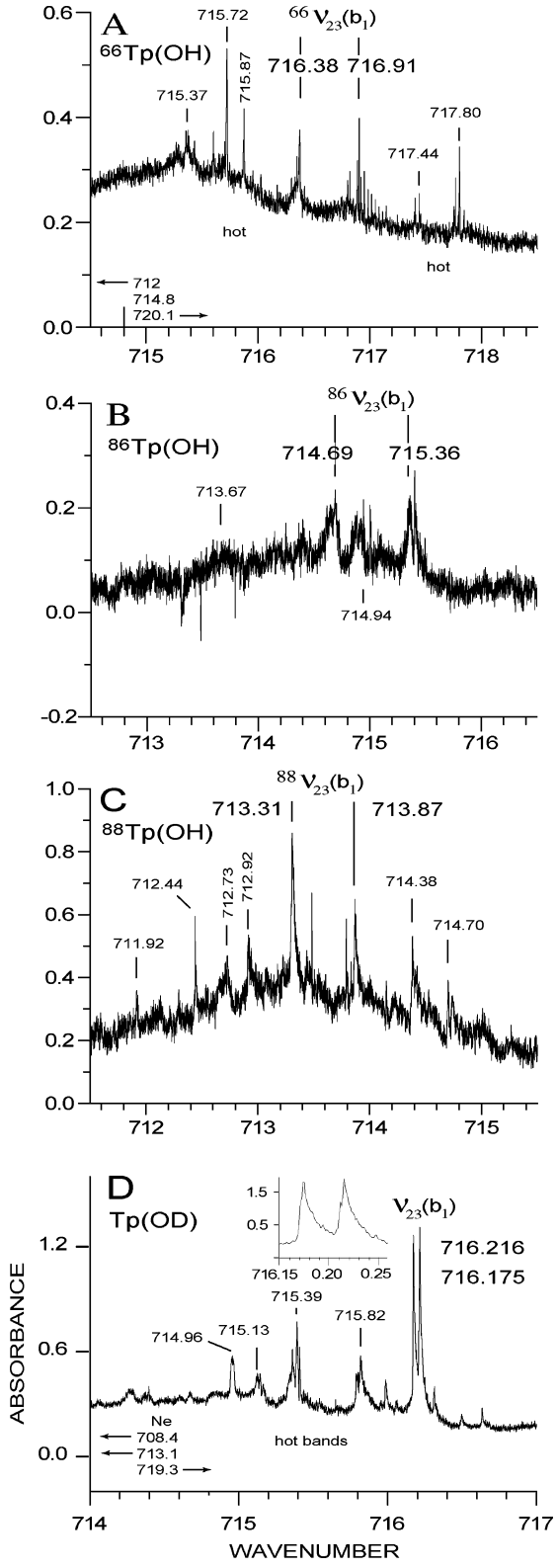

Figure 15. Q spike structures for ${}^{iso}\nu_{23}(b_1)$ of the four Tp isotopomers.

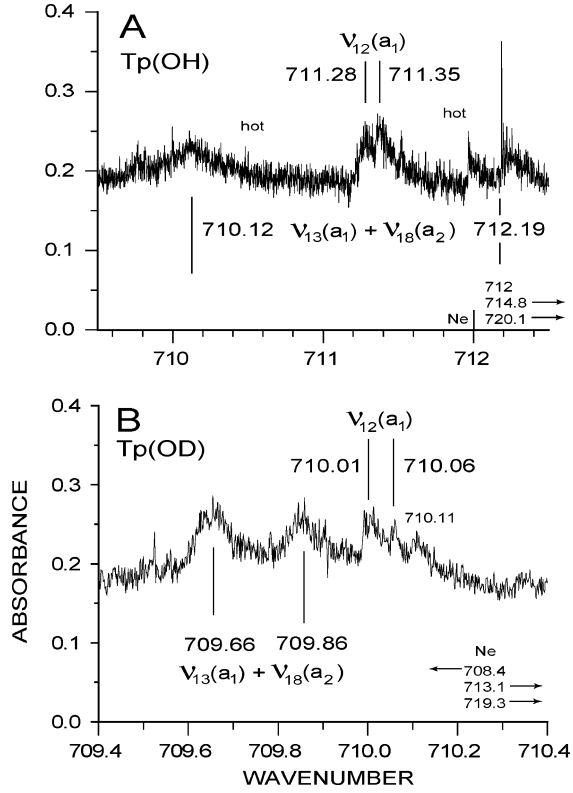

Figure 16. Q spike structure for $\nu_{12}(a_1)$ and $\nu_{13}(a_1)+\nu_{18}(a_2)$ (A_2) of Tp[OH(OD)].

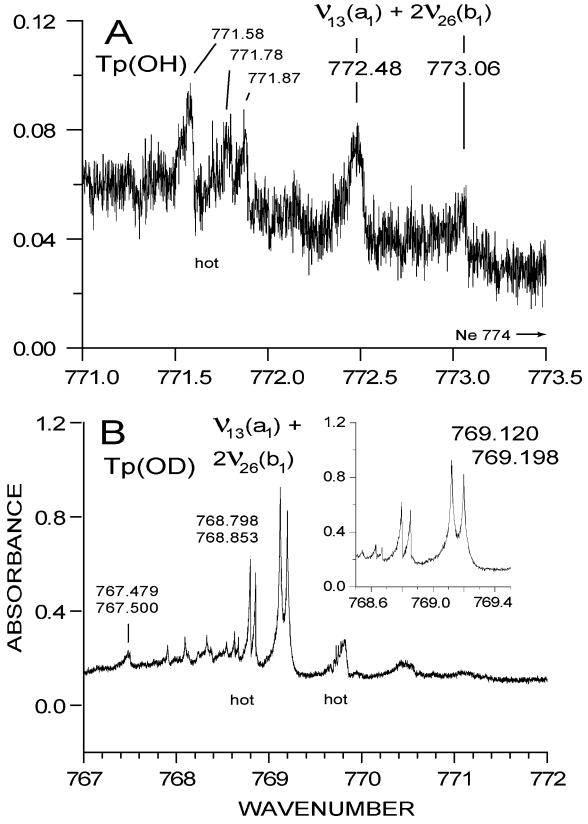

Figure 17. Q spike structure for $\nu_{13}(a_1)+2\nu_{26}(b_1)$ (A_1) of Tp[OH(OD)].

The Ne matrix-induced[31] frequency shifts $\nu_{Ne} - \nu_{gas}$ are 714.8−716.7 = −1.9 cm^{-1} (red) for Tp(OH) and 719.3−716.20 = +3.1 cm^{-1} (blue) for Tp(OD). The 714.8 peak for Ne-isolated Tp(OH) and the 719.3 cm^{-1} peak for Ne-isolated Tp(OD) are both accompanied by adjacent absorptions to suggest, with the gas phase absorbances, probable couplings of $\nu_{23}(b_1)$ to nearby vibrational states. Further, the harmonic MP2/GEN-computed results[15] $\omega_{23} \approx w_{23}^{SP}$ and $Q_{23} \approx Q_{23}^{SP}$ suggest $\Delta_{23} \approx \Delta_0$ rather than the observed (anharmonic) result that $\Delta_{23} > \Delta_0$.

3.13. $\nu_{12}(a_1)$ (Symmetrical Skeletal Breathing). Weak spikes seen near 710 cm^{-1} in Figure 2, panels A and B, are assigned as $\nu_{12}(a_1)$. In Figure 16, panels A and B, the resolved type A doublets produce $^{H}DS_{12} = 0.07 = |^{H}\Delta_{12} - 0.974|$ cm^{-1} and $^{D}DS_{12} = 0.05$ cm^{-1}. The dilated splittings are $^{H}\Delta_{12} = 1.04$ cm^{-1} = 1.07 $^{H}\Delta_0$ and $^{D}\Delta_{12} = 0.10 = 1.96\ \Delta_0$ cm^{-1} as entered in Table 1.

3.14. $\nu_{13}(a_1)+\nu_{18}(a_2)$ (A_2). Figure 16, panels A and B, show widespread doublets assigned as $\nu_{13}(a_1)+\nu_{18}(a_2)$ (A_2). Observed frequencies predict $^{H}\nu_{13+18} = 435.22 + 271 = 706$ cm^{-1} and $^{D}\nu_{13+18} = 429.7 + 271 = 700.7$ cm^{-1}. The doublets produce $^{H}DS_{13+18} = (\Delta_{13+18} + 0.974) = 2.07$ cm^{-1} to give $^{H}\Delta_{13+18}$ = 1.10 cm^{-1} = 1.13 $^{H}\Delta_0$ and $^{D}DS_{13+18} = 0.20 = {}^{D}\Delta_{13+18} + 0.051$ cm^{-1} to give $^{D}\Delta_{13+18} = 0.15$ cm^{-1} = 2.94 $^{D}\Delta_0$ as listed in Table 3. The dilated $\nu_{13} + \nu_{18}$ state splittings are well damped relative to the splittings $^{H,D}\Delta_{13} = 1.76\ ^{H}\Delta_0$ and 6.3 $^{D}\Delta_0$ of their $\nu_{13}(a_1)$ (nominal O···O stretching) constituent.

3.15. $\nu_{13}(a_1) + 2\nu_{26}(b_1)$ (A_1). Figure 2B shows an intense absorbance near 769 cm^{-1} for Tp(OD) that is also intense in Ne and Ar matrix isolation spectra.[15,31] It is seen in Figure 2A to be very weak for Tp(OH). The proposed assignment is ^{D}-$[\nu_{13}(a_1) + 2\nu_{26}(b_1)]$ (A_1). The frequency is calculated as 429.65 + 2(174) = 778 cm^{-1} using observed frequencies. Figure 17B shows the very sharp doublet for Tp(OD) with $^{D}DS_{13+2(26)}$ = 0.078 cm^{-1} = $|^{D}\Delta_{13+2(26)} - 0.051|$ giving $^{D}\Delta_{13+2(26)} = 0.13$ cm^{-1} = 2.5 $^{D}\Delta_0$. The $^{D}\Delta_{13+2(26)}$ splitting is damped relative to $^{D}\Delta_{13} = 6.3\ ^{D}\Delta_0$ through anharmonic couplings between $\nu_{13}(a_1)$ and $\nu_{26}(b_1)$. Similar damping is noted for many hot band states[11] incorporating the $\nu_{19}(a_2)$ or $\nu_{26}(b_1)$ excitations.

Figure 17A shows the weak $\nu_{13}(a_1) + 2\nu_{26}(b_1)$ (A_1) transition of Tp(OH). It lies 16 cm^{-1} to the red of 435.22 + 2(177) = 789 cm^{-1} calculated using observed frequencies. $^{H}DS_{13+2(26)} = |^{H}\Delta_{13+2(26)} - 0.974| = 0.58$ cm^{-1} to give $^{H}\Delta_{13+2(26)} = 1.55$ cm^{-1} = 1.59 $^{H}\Delta_0$ (damped relative to $^{H}\Delta_{13} = 1.76\ ^{H}\Delta_0$). The relative absorbance strengths (and to a lesser extent the frequencies) for transitions in the 700−800 cm^{-1} range of Tp[OH(OD)] suggest strong anharmonic/dynamic rotation-contortion-vibration couplings connect their upper states.

3.16. $\nu_8(a_1) - \nu_{39}(b_2)$. The hot band complex near 763 cm^{-1} was discussed in section 3.7.

3.17. $\nu_{37}(b_2)$ (In-Plane Skeletal Distortion). In earlier work,[15,16] apparent doublets observed for Ne-isolated Tp[OH-(OD)] (cf. Figure 2, panels A and B) were assigned as skeletal contortion doublets with $^{H}\nu_{37}(b_2) = 743.4$, 754 cm^{-1} and $^{D}\nu_{37}$-$(b_2) = 741.4$, 751.3 cm^{-1}. More attractive alternative assignments were not then available for the 754 and 751.3 cm^{-1} peaks, and the proposed large contortional tunneling splittings yielding $^{H,D}DS_{37} \approx 10$ cm^{-1} arose naturally from the utilized ab initio PES and its associated tautomerization mechanism.[16] The present FTIR work abrogates $^{H,D}DS_{37} \approx 10$ cm^{-1} by (a) reassignments for the 754 and 751.3 cm^{-1} peaks of Ne-isolated Tp[OH(OD)] to $\nu_{14}(a_1)+\nu_{25}(b_1)$ (B_1) as described in section 3.1 and by (b) producing the first experimental estimates for the $^{H,D}\Delta_v$ tunneling splittings of the modes incorporating strong O···O stretching activity as described in sections 3.6−3.8. According to conventional wisdom,[5,26,27] these are the heavy atom vibrations expected to most effectively promote the tautomerization reaction. Excluding the OH and OD stretches, Tables 1−4 present spectroscopically estimated state-specific Δ_v values $^{H}\Delta_v < 2$ cm^{-1} and $^{D}\Delta_v < 0.5$ cm^{-1}. The peaks observed for Ne-isolated samples of Tp(OH) at 743.4 cm^{-1} and of Tp(OD) at

741.4 cm^{-1} are entered for $\nu_{37}(b_2)$ in Table 2. No Type B absorption profiles attributable to $\nu_{37}(b_2)$ of the gaseous samples are identifiable in the FTIR spectra (cf. Figures 2, 3, and 5).

4. Multidimensional Tunneling in Tropolone

4.1. Evidence for Multidimensionality. The spectral observations suggest the tautomerization process in Figure 1 utilizes multidimensional processes and widespread dynamical timescales to produce observed tunneling splittings $^{iso}\Delta_v$ dividing into three categories. (a) For vibrations below 800 cm^{-1} the $^{H}\Delta_v/^{H}\Delta_0$ ratios lie between 0.09 and 1.9, and the $^{D}\Delta_v/^{D}\Delta_0$ ratios lie between 0.2 and ~7.5 (Tables 1−4). (b) For fundamentals of Tp(OH) in the 1000−1850 cm^{-1} range,[13] the $^{H}\Delta_v/^{H}\Delta_0$ ratios lie in the narrower 0.85 to 1.15 range. (c) For $\nu_{27}(b_2)$ [OH(OD) stretching] the splitting ratios[10,15,33] are $^{H}\Delta_{27}/^{H}\Delta_0 = 23$ and $^{D}\Delta_{27}/^{D}\Delta_0 = 137$ (Table 2).

The different splitting behaviors observed for the vibrations above and below *ca.* 800 cm^{-1} are attributed to the participation of IVR processes[34−37] in the tautomerization mechanism when $\nu_v > 800$ cm^{-1}. The data infer that for these modes the threshold density of rotation−contortion−vibration background states allowing IVR to occur in Tp has been reached. For discussion, the tunneling splittings Δ_v observed for $\nu_v < 800$ cm^{-1} are labeled $\Delta_v = \Delta_v^0$, with the superscript signifying that no IVR is present. For $\nu_v > 1000$ cm^{-1} IVR contributions to the tautomerization processes are present to some extent. For states allowing the occurrence of IVR processes that are fast on the time scale of the ZP tautomerization rate, the effective PES of the vibrational excited-state is reduced to that of the ZP state with an upward offset in energy. For these vibrations $\Delta_v = \Delta_0$ is observed. For vibrations with slow IVR processes due to low and/or irregular densities of background states, the IVR contributes to observed Δ_v values that are attenuated from the limiting Δ_v^0 values. In principle, the Δ_v^0 values could be determined through quantum mechanical computations. For modes ν_v that inherently promote tunneling, the observed Δ_v values fall in the range $\Delta_v^0 \geq \Delta_v \geq \Delta_0$ and for modes ν_v that inherently damp tunneling they fall in the range $\Delta_v^0 \leq \Delta_v \leq \Delta_0$. With fast IVR the Δ_v values approach Δ_0 and with slow IVR they approach Δ_v^0. Some of the midfrequency fundamentals $^{H}\nu_v$ produce nearly identical observed $^{H}\Delta_v$ splitting values[13] that are not equal to $^{H}\Delta_0$ to suggest the IVR processes acting on the tautomerizations in these states lead to kindred bottleneck configurations. The OH and OD stretching states (cf. Table 2) can be viewed as tautomerizing with the help of IVR contributions to reach multidimensional bottleneck states with $^{H}\Delta_{27} = 22$ $cm^{-1} = 23$ $^{H}\Delta_0$ for Tp(OH) and $^{D}\Delta_{27} = 7$ $cm^{-1} = 137$ $^{D}\Delta_0$ for Tp(OD). These splittings lie in the hierarchies $^{iso}\Delta_{27}^0 \geq {}^{iso}\Delta_{27} \geq {}^{iso}\Delta_0$.

4.2. Corner-Cutting in Tropolone. The spread of the observed $^{iso}\Delta_v$ splittings listed in Tables 1−4 demonstrates the multidimensional quantum character of the intramolecular dynamics of Tp. The data are also expected to reflect the occurrence of deviations between the minimum energy and tunneling pathways leading between the tautomers. Solid experimental and theoretical-computational evidence documenting observable quantum corner-cutting phenomena, with testing by isotopic substitutions, has been accruing for many years.[38−41] Current work carries implications for the mechanisms proposed for enzyme reactions.[42] Evidence for corner-cutting in Tp arises through the splitting ratios $^{iso}\Delta_v/^{iso}\Delta_0$ listed in column 11 in Tables 1−4. These immediately show whether ν_v induces dilation or damping of Δ_v relative to the ZP splitting Δ_0. As used in section 3 and shown in Figure 18A, the ratios correlate the data by obeying $^{66}\Delta_v/^{66}\Delta_0 < {}^{86}\Delta_v/^{86}\Delta_0 < {}^{88}\Delta_v/^{88}\Delta_0$ for the oxygen isotopomers and $^{H}\Delta_v/^{H}\Delta_0 < {}^{D}\Delta_v/^{D}\Delta_0$ for the hydrogen isotopomers. It is argued that the diversity of the H/D isotope effects (cf. bars "d"), and the regularity of the $^{18}O/^{16}O$ isotope effects, provide evidence for isotope-dependent corner-cutting behaviors in the multidimensional state-specific tautomerization mechanisms of Tp.

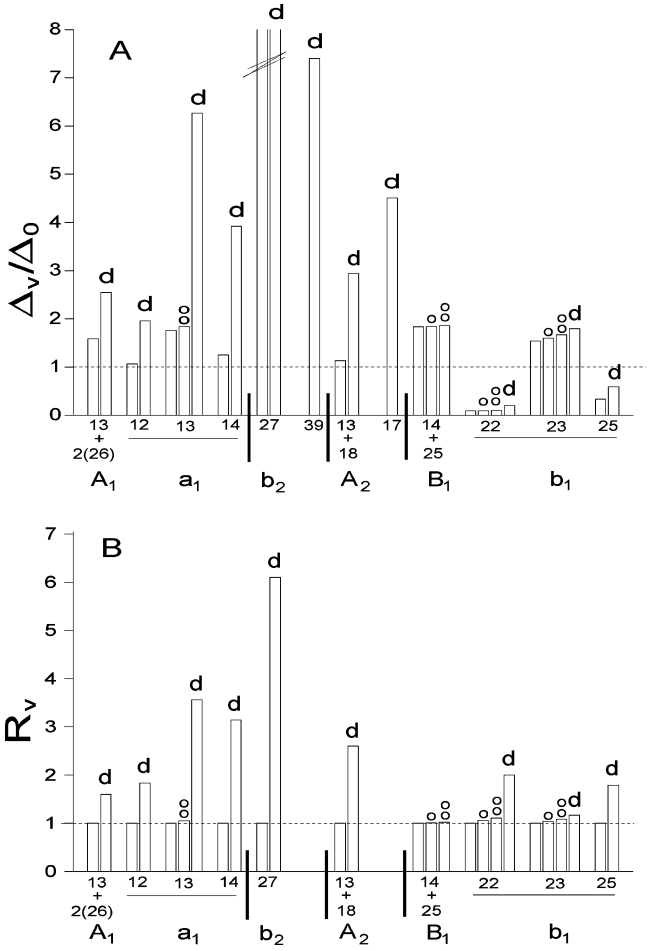

Figure 18. Bar graphs of the tunneling splitting ratio data from columns 11 and 12 of Tables 1−4. The plots support the presence of strong multidimensional and corner-cutting properties in the tautomerization mechanism of tropolone (see text). Note that for each vibration the bar heights increase in the order ^{66}Tp, ^{86}Tp, ^{88}Tp, Tp(OD) [labels −, o, oo, d]. (A) Ratios $\Delta_v/\Delta_0 > 1$ and $\Delta_v/\Delta_0 < 1$ indicate vibrational states which dilate and damp Δ_v relative to Δ_0. (B) The systematic $R_v = (^{iso}\Delta_v/^{66}\Delta_v)/(^{iso}\Delta_0/^{66}\Delta_0) \geq 1.00$ ratios emphasize the greater propensity for corner cutting by the least massive of two compared isotopomers.

An important contribution to the observed behavior is that isotopic substitutions can induce significant changes in the tunneling path lengths, i.e., in the Δ_v values, despite producing only small perturbations of the effective PES for tautomerization. The observed splitting ratio relationships imply there is a straighter, shorter, tunneling path for the less massive isotopomer because the portion of the multidimensional PES rising above the energy of its tunneling state is reduced in comparison to that holding for the more massive isotopomer. Column 12 in Tables 1−4 lists ratios of the column 11 entries as $^{iso}R_v = (^{iso}\Delta_v/^{iso}\Delta_0)/(^{66}\Delta_v/^{66}\Delta_0) = (^{iso}\Delta_v/^{66}\Delta_v)/(^{iso}\Delta_0/^{66}\Delta_0)$. The $^{iso}R_v$ ratios correlate as shown in Figure 18B for the isotopomers. They support the described perspective on corner-cutting through the systematic $^{iso}R_v \geq 1.00$ results observed for all the vibrational states, whether dilating or damping.

A comparatively straighter, shorter, multidimensional tunneling path for Tp(OH) at its high ZP energy value, versus a

swerving, longer, more strongly multidimensional tunneling path for Tp(OD) at its lower ZP energy value, provides a strong drive contributing to the result $^{H}\Delta_0 > {}^{D}\Delta_0$. For Tp, the $^{H}\Delta_0/{}^{D}\Delta_0$ ratio is 0.974/0.051 = 19. Malonaldehyde (MA), with fewer atoms and a lower effective PES barrier than Tp, produces the ratio $^{H}\Delta_0/{}^{D}\Delta_0$= 21.583/2.915[43−45] = 7.40. Theoretical computations[46,47] emphasize the inherent multidimensional nature of the tunneling process in the ZP level of MA.

4.3. Tunneling Splittings for Symmetric Isotopomers of Tropolone. Table 5 presents precise ^{13}C isotope effects observed by Keske et al.[9] on the ZP tunneling splittings of Tp(OH) using the singly labeled isotopomers at natural abundance. There is a 0.4% damping of $^{13}C_5$-Δ_0 {i.e., of Δ_0[^{13}C(5)-Tp(OH)]} relative to normal Δ_0, cf., $^{66}\Delta_0/{}^{13}C_5$-Δ_0 = 0.974/0.970 = 1.004. This important result shows the $^{13}C_5$ atom participates in the tautomerization process of $^{13}C_5$-Tp(OH), despite its remoteness from the H-bond region and its location on the fictive C_2 symmetry axis. The multidimensional tautomerization mechanism for tropolone spans the molecule.

Minor changes to the effective PES for tautomerization accompany isotopic labeling and these drive small tendencies toward the dilation or damping of $^{13}C_5$-Δ_0 relative to $^{12}C_5$-Δ_0. The mass effect of $^{13}C_5$ labeling of Tp(OH) is expected to damp $^{13}C_5$-Δ_0 relative to $^{12}C_5$-Δ_0 to a degree that is beyond other minor effects of the labeling. This is because (a) $^{13}C_5$ replaces $^{12}C_5$ in the multidimensional tautomerization coordinate and (b) the ZP energy of $^{13}C_5$-Tp(OH) is lowered relative to that of $^{12}C_5$-Tp(OH). As discussed above the latter effect induces a lengthening of the tautomerization path length for $^{13}C_5$-Tp(OH) relative to $^{12}C_5$-Tp(OH). The damping effect on the tunneling splitting is magnified by a reduction of PES corner-cutting propensity along the tunneling path for $^{13}C_5$-Tp(OH).

The isotope-induced damping behavior just outlined for $^{13}C_5$-Tp(OH) is paralleled by that for ^{88}Tp(OH) on a scale that is commensurate with the substitution of heavy ^{18}O masses into the H-bond entity itself. The $^{88}\Delta_0$ = 0.83 cm^{-1} value, estimated from Figure 4 and listed in Table 5, produces the ratio $^{66}\Delta_0/{}^{88}\Delta_0$ = 0.974/0.83 = 1.17; that is, $^{88}\Delta_0$ is damped 15% relative to $^{66}\Delta_0 = {}^{H}\Delta_0$ = 0.974 cm^{-1}. Analogous splitting ratios are obtained for the vibrational excited states. For example, consider the entries for $\nu_{13}(a_1)$ (nominal O···O stretching) in columns 10 and 11 of Table 1. The splittings are (a) $^{66}\Delta_{13}$ = 1.71 cm^{-1} = 1.76 $^{66}\Delta_0$, i.e., a dilation of 76% for $^{66}\Delta_{13}$ relative to$^{66}\Delta_0$; and (b) $^{88}\Delta_{13}$ = 1.53 cm^{-1} = 1.84 $^{88}\Delta_0$, i.e. a dilation of 84% for $^{88}\Delta_{13}$ relative to$^{88}\Delta_0$. The isotopic damping of $^{88}\Delta_0$ relative to $^{66}\Delta_0$ is 15%, while in the $\nu_{13}(a_1)$ state the isotopic damping of $^{88}\Delta_{13}$ relative to $^{66}\Delta_{13}$ is 11%. The reduced damping is expected if corner-cutting propensities in the wavefunctions of the $^{66}\nu_{13}$ and $^{88}\nu_{13}$ states, which lie about 430 cm^{-1} above the ZP states, are more nearly the same than are those holding for the ZP states. As seen in Table 2, the deuterium isotope effects are much larger than those for oxygen isotopes, but the same relative tunneling splitting behavior is preserved. The $^{H}\Delta_0/{}^{D}\Delta_0$ = 0.974/0.051 = 19 ratio reflects all ramifications of the substitution of OD for OH on the ZP tunneling splittings. The ZP splitting $^{D}\Delta_0$ = 0.051 cm^{-1} is damped 95% relative to $^{H}\Delta_0$ = 0.974 cm^{-1}, while in the $\nu_{27}(b_2)$ [OH(OD) stretching] state the splitting $^{D}\Delta_{27}$ = 7 cm^{-1} is damped only 68% relative to $^{H}\Delta_{27}$ = 22 cm^{-1}.

4.4. Tunneling Splittings for Asymmetric Isotopomers of Tropolone. An asymmetrically placed single ^{13}C label in Tp, or a single ^{18}O label, breaks the symmetry of this fluxional molecule. The effective PES energy minima for the two tautomer configurations then incorporate different vibrational ZP energies and become unequal. A one-dimensional cut of the effective PES provides the relation $^{as}\Delta_0{}^2 = \Delta_0{}^2 + \delta_0{}^2$ between the three splitting parameters,[14,48,49] where $^{as}\Delta_0$ is the separation between the ZP levels in the asymmetric PES (i.e., the observed ZP splitting). The energy offset between energy minima of the two tautomers is δ_0, and Δ_0 is the splitting between ZP levels of the limiting symmetric PES obtained for $\delta_0 = 0$. Entries listed in Table 5 for $^{13}C_{4(6)}$ and for the other asymmetric isotopomers each include rows for trial Δ_0 estimates obtained by placing arbitrary isotope-induced dampings on the Δ_0 = 0.974 cm^{-1} splitting observed for Tp(OH). Then, given the observed $^{as}\Delta_0$ splitting value, each trial Δ_0 value produces an offset δ_0 between the PES minima through the equation $^{as}\Delta_0{}^2 = \Delta_0{}^2 + \delta_0{}^2$. These δ_0 values are listed in col. 5 of Table 5 for comparison with the independent MO-computed (harmonic) ΔZPE (delta ZP energy) offsets reported by Keske et al.[9] Table 5 contains fixed points for the symmetric Tp(OH), $^{13}C_5$-Tp(OH), ^{18}O,^{18}O-Tp(OH), and asymmetric ^{18}O,^{16}O-Tp(OH) isotopomers. The $^{as}\Delta_0$ = 1.70 cm^{-1} value for ^{86}Tp(OH) was estimated previously[50] from combination differences measured in its $S_1 \rightarrow S_0$ fluorescence excitation spectrum. The energy offset δ_0 = 1.44 cm^{-1} was calculated using $^{as}\Delta_0$ and $^{86}\Delta_0 = 1/2[{}^{88}\Delta_0 + {}^{66}\Delta_0]$ = 0.90 cm^{-1}. The bulleted lines suggest plausible interpolated dampings of the three asymmetric ^{13}C isotopomers between the four fixed point isotopomers.

Table 5 suggests magnitudes for the isotope-induced ZP differences $|{}^{iso}\Delta_0 - {}^{66}\Delta_0|$ are generally smaller than the vibration-induced values $|{}^{H}\Delta_v - {}^{H}\Delta_0|$ listed in Tables 1−4. Table 5 (along with rotational constant data[9]) suggests that intramolecular properties dependent on the C(1) and C(2) atoms joining the two tropolone ring systems play a special role in the effective PES and tautomerization mechanism. According to $^{as}\Delta_0{}^2 = \Delta_0{}^2 + \delta_0{}^2$ the damping of $^{13}C_{2(1)}$-Δ_0 relative to $^{H}\Delta_0$ must be greater than 9% before real numbers are calculated for the energy offset δ_0. Finally, the equation $DS_v = {}^{as}\Delta_v - {}^{as}\Delta_0$ is used with DS_v and Δ_v values from Table 4 and the $^{as}\Delta_0$ = 1.70 cm^{-1} value from Table 5 to provide estimates for δ_v in the three ^{86}Tp(OH) vibrational states for which the $^{86}DS_v$ doublet separations are presently available. The values are δ_{14+25} = 3.1, δ_{22} = 2.3, and δ_{23} = 1.9 cm^{-1}.

5. Concluding Remarks

Changes in the molecular vibrational structure of Tp due to isotopic labeling or to vibrational excitation alter the effective PES determining the state-specific tunneling splitting of the tautomerization process. The effective PES barrier maximum at the SP configuration and the length of the multidimensional tunneling path or swath between the two tautomer minima are certainly two of the premier splitting parameters. In this work the diversity of observed $^{iso}\Delta_v/{}^{iso}\Delta_0$ tunneling splitting ratios and their correlation as $^{light\ iso}\Delta_v/{}^{light\ iso}\Delta_0 < {}^{heavy\ iso}\Delta_v/{}^{heavy\ iso}\Delta_0$ are taken as demonstrating that the tunneling in Tp isotopomers has a strong multidimensional character with significant state-specific corner-cutting propensities. A tautomerization tunneling path must thread its way through features of a multidimensional effective PES that is subject to adjustment upon vibrational excitation and/or isotopic labeling. The propensity for path-shortening corner-cutting increases as the ZP or excited vibrational energy of the examined tunneling state is raised above the floor set by the reference state.

Columns 11 and 12 in Tables 1−4 show the effects of vibrational excitation and of isotopic labeling on $^{iso}\Delta_v/{}^{iso}\Delta_0$ ratios (column 11), and on the ratios of these values to $^{66}\Delta_v/{}^{66}\Delta_0$ ($^{iso}R_v$, column 12). The Δ_v/Δ_0 ratios provide an immediate measure

of the damping or dilation of the splitting Δ_v relative to the ZP value Δ_0 for each isotopomer. The $^{iso}R_v = (^{iso}\Delta_v/^{66}\Delta_v)/(^{iso}\Delta_0/^{66}\Delta_0)$ ratios provide a related measure emphasizing the importance of multidimensional corner-cutting for the tunneling pathways. The ratios listed in columns 11 and 12 of Tables 1−4 are displayed in Figure 18 to emphasize the diversity of H/D effects and the relative systematics of $^{18}O/^{16}O$ entries. The correlations seen in Figure 18 were useful for interpreting the data for spectral tunneling doublets.

Acknowledgment. The high-resolution FTIR data reported in this paper were recorded at the W. R. Wiley Environmental Molecular Sciences Laboratory, a national scientific user facility sponsored by the Department of Energy's Office of Biological and Environmental Research and located at Pacific Northwest National Laboratory. Pacific Northwest National Laboratory is operated for the U.S. Department of Energy by Battelle under Contract DE-AC06-76RLO1830.

References and Notes

(1) Alves, A. C. P.; Hollas, J. M. *Mol. Phys.* **1972**, *23*, 927.
(2) Alves, A. C. P.; Hollas, J. M. *Mol. Phys.* **1973**, *25*, 1305.
(3) Redington, R. L.; Chen, Y.; Scherer, G. J.; Field, R. W. *J. Chem. Phys.* **1988**, *88*, 627.
(4) Sekiya, H.; Nagashima, Y.; Nishimura, Y. *Bull. Chem. Soc. Jpn.* **1989**, *62*, 3229.
(5) Sekiya, H.; Nagashima, Y.; Nishimura, Y. *J. Chem. Phys.* **1990**, *92*, 5761.
(6) Tanaka, K.; Honjo, H.; Tanaka, T.; Kohguchi, H.; Ohshima, Y.; Endo, Y. *J. Chem. Phys.* **1999**, *110*, 1969.
(7) Bracamonte, A. E.; Vaccaro, P. H. *J. Chem. Phys.* **2003**, *119*, 997.
(8) Bracamonte, A. E.; Vaccaro, P. H. *J. Chem. Phys.* **2004**, *120*, 4638.
(9) Keske, J. C.; Lin, W.; Pringle, W. C.; Novick, S. E.; Blake, T. A.; Plusquellic, D. F. *J. Chem. Phys.* **2006**, *124*, 074309.
(10) Frost, R. K.; Hagemeister, F. C.; Arrington, C. A.; Zwier, T. S.; Jordan, K. D. *J. Chem. Phys.* **1996**, *105*, 2595.
(11) Redington, R. L.; Sams, R. L. *J. Phys. Chem. A* **2002**, *106*, 7494.
(12) Redington, R. L.; Sams, R. L. *Chem. Phys.* **2002**, *283*, 135.
(13) Redington, R. L.; Redington, T. E.; Sams, R. L. *J. Phys. Chem. A* **2006**, *110*, 9633.
(14) Redington, R. L.; Redington, T. E.; Blake, T. A.; Sams, R. L.; Johnson, T. J. *J. Chem. Phys.* **2005**, *122*, 224311.
(15) Redington, R. L.; Redington, T. E.; Montgomery, J. M. *J. Chem. Phys.* **2000**, *113*, 2304.
(16) Redington, R. L. *J. Chem. Phys.* **2000**, *113*, 2319.
(17) Vener, M. V.; Scheiner, S.; Sokolov, N. D. *J. Chem. Phys.* **1994**, *101*, 9755.
(18) Smedarchina, Z.; Siebrand, W.; Zgierski, M. Z. *J. Chem. Phys.* **1996**, *104*, 1203.
(19) Takada, S.; Nakamura, H. *J. Chem. Phys.* **1995**, *102*, 3977.
(20) Wójcik, M. J.; Nakamura, H.; Iwata, S.; Wiktor, T. *J. Chem. Phys.* **2000**, *112*, 6322.
(21) Paz, J. J.; Moreno, M.; Lluch, J. M. *J. Chem. Phys.* **1995**, *103*, 353.
(22) Guo, Y.; Sewell, T. D.; Thompson, D. L. *J. Phys. Chem. A* **1998**, *102*, 5040.
(23) Giese, K.; Kühn, O. *J. Chem. Phys.* **2005**, *123*, 054315.
(24) Tautermann, C. S.; Voegele, A. F.; Loerting, T.; Liedl, K. R. *J. Chem. Phys.* **2002**, *117*, 1967.
(25) Wójcik, M. J.; Boczar, M.; Stoma, M. *Int. J. Quant. Chem.* **1999**, *73*, 275.
(26) Redington, R. L. in Vol. 1, *Hydrogen Transfer Reactions*; Hynes, J. T., Klinman, J. P., Limbach, H. H., Schowen, R. L., Eds.; Wiley−VCH Verlag GmbH & Co. KGaA: Weinheim, Germany, 2007.
(27) Giese, K.; Petković, M.; Naundorf, H.; Kühn, O. *Phys. Rep.* **2006**, *430*, 211.
(28) Frisch, M. J.; Trucks, G. W.; Schlegel, H. B.; Scuseria, G. E.; Robb, M. A.; Cheeseman, J. R.; Zakrzewski, V. G.; Montgomery, J. A.; Stratmann, R. E.; Burant, J. C.; Dapprich, S.; Millam, J. M.; Daniels, A. D.; Kudin, K. N.; Strain, M. C.; Farkas, O.; Tomasi, J.; Barone, V.; Cossi, M.; Cammi, R.; Mennucci, B.; Pomelli, C.; Adamo, C.; Clifford, S.; Ochterski, J.; Petersson, G. A.; Ayala, P. Y.; Cui, Q.; Morokuma, K.; Malick, D. K.; Rabuck, A. D.; Raghavachari, K.; Forseman, J. B.; Cioslowski, J.; Ortiz, J. V.; Stefanov, B. B.; Liu, G.; Liashenko, A.; Piskorz, P.; Komaromi, I.; Gomperts, R.; Martin, R. L.; Fox, D. J.; Keith, T.; Al-Laham, M. A.; Peng, C. Y.; Nanayakkara, A.; Gonzalez, C.; Challacombe, M.; Gill, P. M. W.; Johnson, B. G.; Chen, W.; Wong, M. W.; Andres, J. L.; Head-Gordon, M.; Replogle, E. S.; Pople, J. A. *Gaussian 98*, revision A.6; Gaussian, Inc.: Pittsburgh, PA, 1998.
(29) Burns, L. A.; Murdock, D.; Vaccaro, P. H. *J. Chem. Phys.* **2006**, *124*, 204307.
(30) Rostkowska, H.; Lapinski, L.; Nowak, M. J.; Adamowicz, L. *Int. J. Quantum Chem.* **2002**, *90*, 1163.
(31) Redington, R. L.; Redington, T. E. *J. Mol. Spectrosc.* **1979**, *78*, 229.
(32) Alves, A. C. P.; Hollas, J. M.; Musa, H.; Ridley, T. *J. Mol. Spectrosc.* **1985**, *109*, 99.
(33) Redington, R. L.; Redington, T. E. *J. Chem. Phys.* **2005**, *122*, 124304.
(34) Lehmann, K. K.; Scoles, G.; Pate, B. H. *Annu. Rev. Phys. Chem.* **1994**, *45*, 241.
(35) Keske, J. C.; Pate, B. H. *Annu. Rev. Phys. Chem.* **2000**, *51*, 323.
(36) Callegari, A.; Pearman, R.; Choi, S.; Engels, P.; Srivastava, H.; Gruebele, M.; Lehmann, K. K.; Scoles, G. *J. Chem. Phys.* **2003**, *101*, 551.
(37) Callegari, A.; Merker, U.; Engels, P.; Srivastava, H. K.; Lehmann, K. K.; Scoles, G. J. *J Chem. Phys.* **2000**, *113*, 10583.
(38) Miller, W. H. *Chem. Rev.* **1987**, *87*, 19.
(39) Schatz, G. C. *Chem. Rev.* **1987**, *87*, 81.
(40) Hartke, B.; Manz, J. *J. Am. Chem. Soc.* **1988**, *110*, 3063.
(41) Truhlar, D. G.; Gordon, M. S. *Science* **1990**, *249*, 491.
(42) Pu, J.; Gao, J.; Truhlar, D. G. *Chem. Rev.* **2006**, *106*, 3140.
(43) Firth, D. W.; Beyer, K.; Dvorak, M. A.; Reeve, S. W.; Grushow, A.; Leopold, K. R. *J. Chem. Phys.* **1991**, *94*, 1812.
(44) Baba, T.; Tanaka, T.; Morino, I.; Yamada, K. M. T.; Tanaka, K. *J. Chem. Phys.* **1999**, *110*, 4131.
(45) Baughcum, S. L.; Duerst, R. W.; Rowe, W. F.; Smith, Z.; Wilson, E. G. *J. Am. Chem. Soc.* **1981**, *103*, 6296.
(46) Mil'nikov, G. V.; Nakamura, H. *J. Chem. Phys.* **2001**, *115*, 6881.
(47) Mil'nikov, G. V.; Yagi, K.; Taketsugu, T.; Nakamura, H.; Hirao, K. *J. Chem. Phys.* **2004**, *120*, 5036.
(48) Hameka, H. F.; de la Vega, J. R. *J. Am. Chem. Soc.* **1984**, *106*, 7703.
(49) Skinner, J. L.; Trommsdorff, H. P. *J. Chem. Phys.* **1988**, *89*, 897.
(50) Redington, R. L.; Redington, T. E.; Hunter, M. A.; Field, R. W. *J. Chem. Phys.* **1990**, *92*, 6456.